Chem Soc Rev

Silica-based nanocapsules: synthesis, structure control, and biomedical applications

Journal:	*Chemical Society Reviews*
Manuscript ID:	CS-TRV-06-2014-000199.R2
Article Type:	Review Article
Date Submitted by the Author:	20-Sep-2014
Complete List of Authors:	Zhang, Yu; National University of Singapore, Department of Materials Science and Engineering Hsu, Benedict; NUS Graduate School for Integrative Science and Engineering, Ren, Changliang; Institute of Materials Research and Engineering, Li, Xu; Institute of Materials Research and Engineering, Wang, John; National University of Singapore, Department of Materials Science and Engineering

Chem Soc Rev

RSCPublishing

REVIEW ARTICLE

Silica-based nanocapsules: synthesis, structure control and biomedical applications

Cite this: DOI: 10.1039/x0xx00000x

Yu Zhang,[a] Benedict You Wei Hsu,[b] Changliang Ren,[c] Xu Li*[c] and John Wang*[ab]

Received 11th June 2014,
Accepted 00th September 2014

DOI: 10.1039/x0xx00000x

www.rsc.org/

Synergistically combining the merits of silica (*e.g.*, mechanical robustness, biocompatibility and great versatility in surface functionalization) and capsular configurations (*e.g.*, large inner cavity, low density and favourable colloidal properties), silica-based nanocapsules (SNCs) with a size cutoff of ~100 nm have gained a growing interest in encapsulating bioactive molecules for bioimaging and controlled delivery applications. Within this context, this review provides a comprehensive overview of the synthetic strategies, structural control and biomedical applications of SNCs. Special emphases are placed on size control at the nanoscale and material composition manipulation of each strategy and the newly emerging synthetic strategies. The applications of SNCs in bioimaging/diagnosis and drug delivery/therapy and the structure engineering that is critically important for the bio-performance of SNCs are also addressed in this review.

1 Introduction

Capsules are defined as vesicular or "reservoir" systems in which hollow or soft material-filled cavities are surrounded by a shell of solid materials.[1–3] With the fascinating structural features such as a large inner cavity, low density and favourable colloidal behaviour, capsules have been widely explored to modulate both chemical and physical characteristics of materials that enhance the overall stability in various environments when compared to their solid counterparts, as well as to increase the active area and pore volume for applications in catalysis, adsorption and energy storage.[1–4] In addition, they are extremely useful to encapsulate various substances within their confined cavities so as to exhibit special optical, electrical, magnetic, chemical and biological properties.[1–3] In particular, polymeric capsules of a wide variety of morphologies (*e.g.*, micelles and vesicles) and compositions (*e.g.*, polysaccharides, polypeptides, and amphiphilic fullerene derivatives), liposomes and inorganic hollow spheres have been demonstrated to be robust and tunable encapsulants for the immobilization of functional agents such as drugs, dyes, enzymes, genes, peptides, and other bioactive molecules.[2,5–8] This has even driven the commercialization of some of the products (*e.g.*, Doxil) in medicine and diagnosis.

Silica capsules are ideal candidates as encapsulants for biomedical usage because they combine the merits of silica and capsular nanostructure. Silica is a non-toxic and biocompatible material.[1] It is "generally recognized as safe" (GRAS) by the US Food and Drug Administration (FDA), as demonstrated by its common usage in the food additives and vitamin supplements. It also possesses the advantages of being low cost in production, mechanical and chemical stability, and optical transparency. The surface of silica is largely rich in hydroxyl groups, which renders it to be intrinsically hydrophilic and favourable for colloidal stability. Additionally, the silica surface can be easily modified by various functional moieties such as polymers and antibodies *via* well-established siloxane chemistry to gain multifunctionality.[1,8]

Since the pioneering work on templating synthesis of silica capsules from 1996 to 1998,[9–12] a variety of synthesis paradigms have been employed to prepare varying types of silica capsules. They have dramatically expanded the range of silica capsules in sizes, shapes, and surface chemistry which has in turn catalysed new applications and fundamental research on silica capsules. In particular, silica-based nanocapsules (SNCs) on a truly nanoscale size (*i.e.*, <100 nm) are gaining increasing attention, especially in the field of biomedical research. This is because the size cutoff of ~100 nm offers considerable advantages such as reducing the reticuloendothelial system (RES) capture, prolonging blood circulation time, enhancing extravasation into targeted sites, increasing cellular uptake, and facilitating barrier penetration. A large number of SNCs have thus been developed in association with the advances of conventional templating synthesis and the emergence of new synthetic strategies (*e.g.*, single micelle templating). The resulting SNCs have been extensively explored in various biomedical applications such as bioimaging/diagnosis and drug delivery/therapy. Within this context, this article reviews recent advances in the synthetic strategies, structural control of SNCs and their biomedical applications.

It is noted that although a number of reviews with regard to the synthesis of various silica nanostructures such as spheres, core/shells, and mesoporous silica, and/or their applications have already been published,[8,13,14] research on the synthesis and biomedical applications of SNCs with a hollow or hybrid capsular structure and in particular on a truly nanoscale size

(*i.e.*, <100 nm) has never been specifically and properly reviewed. To keep the review down to a manageable level, three dimensional porous silica (*e.g.* silica nanofoams), micro/meso/macroporous silica and silica nanotubes are not considered in this review.

In the first section of this review, we present a comprehensive overview of the synthetic strategies, which are categorized into cavity-generating (*e.g.*, hard templating, soft templating and template-free) and shell-forming (*e.g.*, stöber, reverse microemulsion and supramolecular-templated deposition). Special emphasis is placed on the key points of each strategy for a more precise control of the nanoscale size and material composition. Besides, the single-micelle templating approach is highlighted due to its effectiveness on fabricating SNCs. Next we address the structure control of SNCs in terms of particle size, level of shell porosity, cavity topology, cavity content, and surface functionality that are critical for their bio-performance. This is followed by the section that details a survey of SNCs as an excellent encapsulant to load a wide variety of bioactive agents for a broad range of biomedical applications. Finally, we conclude this review with some perspectives on the future research and development of SNCs.

2 Design and synthetic strategies of silica-based nanocapsules

The development of SNCs generally involves three major steps, as illustrated in Figure 1: (i) preparation of a nanosized template; (ii) formation of a silica-based shell on the template by depositing silica precursors (salts or alkoxides) onto the surface of the template; and followed by (iii) template removal through either calcination at high temperature or dissolution with a suitable solvent to generate a cavity inside the shell. In this review, the design and synthesis strategies of SNCs are categorized into cavity-generating and shell-forming respectively. More specifically, cavity-generating strategies include hard templating, soft templating, and the newly emerging template-free syntheses. In this regard, a wide panel of hard (*i.e.*, rigid solid) templates such as polymer latex and inorganic nanoparticles (NPs) and soft (*i.e.*, flexible solid, liquid, and gaseous) templates such as (micro)emulsion droplets, vesicles, micelles, polymer aggregates and gas bubbles have been employed to generate the cavity in SNCs. On the other hand, shell-forming strategies include stöber, reverse microemulsion, and supramolecular-templated deposition methods. In this section we present an overview of these synthetic strategies emphasizing on the aspects of size control at nanoscale and silica composition control.

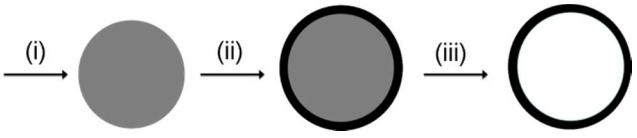

Figure 1 Schematic illustration of the general steps for the formation of SNCs: (i) preparation of a nanosized template; (ii) deposition of a silica-based shell on the template; and (iii) template removal to generate a cavity inside the shell.

2.1 Cavity-generating strategies

To date, both hard and soft templating have been widely explored for the cavity generation in inorganic (silica and non-silica) hollow spheres. In general, when hard templates are employed, the templates must be eliminated eventually to leave behind a hollow shell. The shape and cavity size of the thus achieved hollow products are determined by the hard templates, which typically are monodisperse and have a well-defined morphology. However, removal of the templates through either thermal calcination or chemical etching may be uneconomic, time-consuming, and sometimes involves the utilization of toxic chemicals that can be harmful to the surrounding environment. As for the soft templating synthesis, although it is relatively easier to remove the templates, the as-prepared hollow products usually suffer from ill-defined morphologies and poor monodispersity due to the deformability and wide size distribution of the soft templates. Nonetheless, the recent emergence of single micelle templating, as well as the template-free approach, has been effective on synthesizing SNCs and thus will be highlighted in this section.

2.1.1 Hard templating

In the conventional hard templating synthesis, polymer (*e.g.*, polystyrene (PS)) latex beads and inorganic NPs (*e.g.*, SiO_2 particles) are the most commonly used templates for generating cavity owing to their easy preparation and well-tunable size and morphology. In the PS templating approach, it can be traced back to Caruso's seminal paper in 1998.[11] In this work, hollow SiO_2 particles in the size range of 720–1000 nm were synthesized by using PS templating combined with layer-by-layer (LBL) sequential deposition of oppositely charged SiO_2 NPs and polyelectrolytes. Despite its versatility, the PS templating approach has been generally employed to fabricate relatively large hollow particles; the diameters of which is determined by the size of the PS templates and is typically in the submicron- and micrometer range. In order to develop nanosized hollow silica, two crucial factors need to be satisfied: (i) nanosized PS templates, and (ii) proper surface functionalization of PS templates which is essential for obtaining a good coverage and uniform coating of silica in a later shell-forming process.[15] The surface functional groups on nanosized PS templates that show strong affinity to silica include neutral or slightly positively charged amine ($–NH_2$), negatively charged sulfate ($–SO_4^-$), and zwitterionic $–NH_3^+$/$–COO^-$ groups (Figure 2).[15–19] These functional groups are typically anchored to the PS template surface by co-polymerization of styrene monomer with functional co-monomer bearing the specific functional groups of interest.

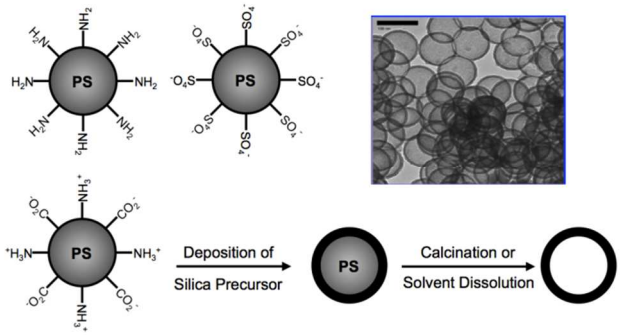

Figure 2 Schematic illustration of the formation of SNCs by using functionalized PS templates. The scale bar in the TEM image is 100 nm. (Adapted from Ref. 15 with permission from The Royal Society of Chemistry. Reprinted with permission from ref. 16. Copyright 2008 American Chemical Society.)

In recent years, inorganic NPs have emerged as a new and promising class of hard templates for the fabrication of SNCs because they can be made very small (<100 nm) and highly monodisperse. Indeed, different inorganic NPs, including iron oxides (Fe_2O_3,[20–22] and Fe_3O_4[23,24]), $CaCO_3$,[25–30] PbS,[31] and Au NPs,[32,33] have been investigated for such purpose. These materials are selected because they can be dissolved in particular acids (*e.g.*, hydrochloric acid,[21–29] nitric acid,[31,34] and oxalic acid[20]), alkalis (*e.g.*, ammonia[34]), or an appropriate solvent (*e.g.*, cyanide[33]) in which silica is not soluble. Thus, it allows for a selective dissolution of the templates without affecting the silica shell.

2.1.2 Soft templating

The strength of the hard templating synthesis of SNCs lies in the precise control over size and monodispersity. Nonetheless, it generally suffers from several drawbacks. For example, the choice of available hard templates is rather limited due to the difficulty in tuning the dimensions of nanosized PS, complicated surface functionalization process, and high cost of inorganic NPs. Post-loading of the hollow cavity or *in situ* encapsulation with bioactive compounds (*e.g.*, therapeutics drugs and contrast agents) is also challenging, and these constrain their biomedical applications. In this regard, templating against soft templates are very attractive and have been investigated extensively for the fabrication of SNCs because of the following advantages: simplified synthesis procedures (*i.e.*, particularly with one-pot synthesis approach), as well as a more gentle template removal process at room temperature and with common solvents such as ethanol. More importantly it offers the possibility of *in situ* encapsulation of bioactive compounds during the synthesis of the nanocapsules, thus avoiding the complicated re-filling step. A number of soft templates have been examined for this purpose, including for example microemulsion droplets, vesicles, micelles, polymer aggregates, and gas bubbles. In this section, the use of each typical type of soft templates for the preparation of SNCs is addressed, with an emphasis on the usage of micelles as templates.

Microemulsion templating

Microemulsion is defined as an optically isotropic, thermodynamically stable and transparent (or translucent) system composed of two immiscible liquid phases (water and oil), surfactant, and usually co-surfactant. One liquid phase (*i.e.*, the dispersed phase or droplet) is dispersed in the other (*i.e.*, the continuous phase) to form droplet sizes in the order of 20–200 nm. A monolayer of surfactant molecules is self-assembled at the interface between the droplet and the continuous phase to facilitate the dispersion process by lowering the interfacial tension while the size, shape, and curvature of the droplets can be tuned by the surfactant type and structure. A microemulsion can be further classified as direct (oil-in-water, O/W), reverse (water-in-oil, W/O), or bicontinuous systems.

As to the microemulsion templating synthesis of hollow silica, the basic idea is to grow the silica shell exclusively at the interfacial region between the droplets and the continuous phase. In this regard, surfactants or co-surfactants should have good affinity to the silica precursors either through electrostatic interaction or hydrogen bonding. The liquid droplets, which act as the cavity-generating templates, can then be easily removed by a gentle evaporation or dissolution in mild solvents such as water and ethanol after the shell formation.

Compared to hard templates, this method allows for easy template removal and incorporation of a wide range of functional molecules (hydrophilic and hydrophobic) due to the presence of both hydrophobic and hydrophilic domains. Hence, it is particularly attractive in drug delivery and pharmaceutical applications. However, it is rather challenging to obtain uniform droplets with size smaller than 100 nm. This is because the droplets constantly move, collide and exchange with each other to cause droplet coalescence and Ostwald ripening, As a result, silica capsules derived from microemulsion templating is usually larger than 200 nm in size. They also exhibit broad size distributions or serious interparticle aggregation, which are great handicaps for their biological application.

Over the years, several reports have described how both direct and reverse microemulsion systems are used for the preparation of monodisperse SNCs.[35–37] As compared to the direct microemulsion, the reverse microemulsion demonstrates better capability to produce monodisperse SNCs with sizes in the sub-50 nm range. This is because the growth of silica is confined inside the water droplet. Thus, it does not interfere with the functioning of surfactant molecules, which are located at the interface of the W/O droplet, to prevent the SNCs from sticking together.[35,37] Nevertheless, in most cases, the use of single-hydrocarbon chain surfactants (*e.g.*, Triton X-100,[35] cetyltrimethylammonium bromide (CTAB),[36] and Tween-80[37]) alone is unable to reduce the interfacial tension sufficiently to form a stable microemulsion.[35–37] One effective way to improve the system stability is to introduce a co-surfactant so as to reduce the interfacial tension and ensure sufficient flexibility of the interface. As a second surface-active species, the co-surfactant can be either another surfactant (*e.g.*, lecithin[37]) or a medium sized aliphatic alcohol (*e.g.*, hexanol),[35,36] Another effective way to fortify the microemulsion droplets is to introduce a cross-linkable surfactant (*e.g.*, octadecyltrimethoxysilane (C_{18}TMS)[37]).

Vesicle templating

Amphiphilic surfactants or block copolymers with clearly distinct hydrophobic and hydrophilic groups are able to self-assemble into vesicles. Vesicles are hollow spheres with bilayer structured walls. The bilayers arise due to an inward orientation of the hydrophobic blocks and an outward protrusion of the hydrophilic blocks into the water-filled interior cavity as well as the external medium. With an inherent hollow structure and rich morphologies, vesicles are of particular interest as templates for the synthesis of SNCs. Various factors such as the type of surfactants, the components of surfactant mixtures, temperature, pH, or stirring rates have been delicately adjusted to determine the dimensions, morphology and stability of vesicles.[38–40]

Pinnavaia and co-workers were among the first who have successfully synthesized SNCs by using vesicle templating.[12] In their study, vesicles were prepared from neutral gemini surfactants of $C_nH_{2n+1}NH(CH_2)_2NH_2$ (n = 10, 12, 14) and the silica precursor of tetraethoxysilane (TEOS). Due to the penetration of TEOS into the vesicle layers to interact with the gemini through hydrogen bonding, as-prepared hollow silica exhibited ultrahigh thermal (1000 ^oC) and hydrothermal stabilities. However, the hollow silica was actually a mixture of single-walled hollow silica (SWHS) and multi-walled hollow silica (MWHS) with very wide size distributions that ranges

Table 1 A brief summary of vesicle templating synthesis of SNCs.

Templating agent		Morphology	Particle size (nm)[a]	Shell thickness (nm)[a]	Ref.
Gemini surfactant	$C_nH_{2n+1}NH(CH_2)_2NH_2$	SWHS + MWHS	SWHS: 20–125; MWHS: 33–1400	SWHS: 3; MWHS: 7–70	12
	$C_nH_{2n+1}NH(CH_2)_mNH_2$	SWHS	18–37	2–3	41
		MWHS	18–100	8–40	
Catanionic surfactant	CTAB/PFOA	*h*-MS-MWHS	(100–300) × (50–150)	~25–50	43
		MWHS	70–200	~25–50	
		SWHS	60–120	~10	
Cationic surfactant	DODAB	SWHS	50–200	6–9[b]	42
	DDAB[c]	MWHS	30–50	10	40
Nonionic surfactant	PEO_{20}-PPO_{70}-PEO_{20} (P123)[c]	SWHS	50–150	5	38
Partially fluorinated surfactant	HFDePC	*d*-MS-SWHS	~100	10–20	39
	FC4 + CTAB	*h*-MS-MWHS	70–180	20	45
	F_8H_{10}	MWHS	50–120	15–20	44
Reactive block copolymer	PEO-PTMSPMA	SWHS	45.6 ± 12.1	16.9 ± 2.5	46

[a] Determined by TEM. [b] Determined by DLS. [c] DDAB: didodecyldimethylammonium bromide; P123: poly(ethylene oxide)$_{20}$-*block*-poly(propyl oxide)$_{70}$-*block*-poly(ethylene oxide)$_{20}$ (PEO_{20}-PPO_{70}-PEO_{20}).

from tens of nanometer to 1.4 micrometer. Nonetheless, in a later work done by the same group,[41] smaller SWHS (<40 nm) and MWHS (<100 nm) were successfully synthesized due to a proper balance of the hydrophilic and hydrophobic interactions during the assembly process of gemini surfactants.

Hubert *et al.* reported the first successful synthesis of SWHS by using a cationic surfactant of dioctadecyldimethylammonium bromide (DODAB).[42] Alternatively, catanionic surfactant, which is a cationic-anionic surfactant mixture, represents an interesting class of vesicle templates. Such catanionic mixture initiates the formation of bilayer structures with high stiffness owing to the strong electrostatic interaction between the positively and negatively charged head groups.[43] A catanionic mixture of cationic CTAB and anionic perfluorooctanoic acid (PFOA) have been employed to direct the formation of SWHS, MWHS, and MWHS with a mesoporous shell (MS-MWHS), respectively.[43] In addition, non-ionic PEO-based triblock copolymers has also been applied to the formation of SWHS by delicately adjusting pH and temperature in salted buffer solutions.[38]

Compared to hydrogenated surfactants, partially fluorinated surfactants are more prone to forming stable vesicles because their fluorocarbon and hydrocarbon segments can increase the elasticity and flexibility of the bilayer respectively.[39,44,45] Rankin's groups first reported the use of 1H, 1H, 2H, 2H-perfluorodecylpyridinium chloride (HFDePC) to synthesize SWHS with only a single layer of mesopores in the silica wall.[39] Because of the stability of the fluorocarbon bilayers, they are used to direct the formation of organic-inorganic hybrid hollow silica from ethylene-bridged silanes. Ethane-silica of MSHS and MWHS have been synthesized using $C_3F_7O(CFCF_3CF_2O)_2CFCF_3$-$CONH(CH_2)_3N^+(C_2H_5)_2CH_3I^-$ (FC4) and 1-(10-perfluorooctyldecyl)pyridinium bromide monohydrate (F_8H_{10}) respectively.[44,45] This strategy is desirable because there is a rather uniform distribution of the organic ethylene-bridging groups within the silica framework. However, long-chain bridged silanes, such as octylene-bridged silane, were unsuccessful to achieve stable hollow particles. This is due to the flexibility of the walls which makes the particles susceptible to collapse upon drying. Additionally, the introduction of an amine group into the bridging chain could also prevent the formation of hollow structures, either because the amine has accelerated the hydrolysis process or increased the polarity of the bridging chain.[44]

Alternatively, Du *et al.* reported a successful synthesis of organic-inorganic hybrid hollow silica by using a home-designed amphiphilic diblock copolymer of PEO-*block*-poly(3-(trimethoxysilyl) propyl methacrylate) (PEO-PTMSPMA), which bears the reactive trimethoxysilane groups in one segment of the polymer to function as the silica precursor.[46]

Table 1 presents a summary of the SNCs synthesized by vesicle templating, along with their templating agents, morphologies, and particle size and shell thickness. Hollow silica with a mesoporous shell is denoted as *x*-MS-SWHS or *x*-MS-MWHS, where *x* = *d* or *h* corresponding to disordered or hexagonal mesoporous shells, respectively.

As summarized in Table 1, with only a few exceptions, majority of the as-prepared silica have a wide distribution of sizes varying from nanometers to sub-micrometers and ill-defined morphologies. Hence, it is generally challenging to control the size of hollow silica to be fully below 100 nm through the vesicle templating approach. In most cases, SNCs are likely to coexist with hollow silica (>100 nm in size) in the same product, sometimes even constitute only a small fraction of the entirety. This can be ascribed to the characteristics of templating vesicles, which are broad in size span, as well as the bilayer shells, which are fragile and prone to collapse as conditions change.[1]

In addition, the resultant SWHS tend to possess a very thin wall in the range of 2–10 nm. Thickness of the wall can be increased if block copolymers of large molecular weight are used as vesicle templates.[46] On the other hand, for MWHS derived from multilamellar vesicles, the wall thickness is determined by the thickness of each layer and layer spacing.

Single micelle templating

Although the liquid characteristics of microemulsion droplets and the inherent hollow cavity of vesicles provide important advantages for the loading of drug and imaging contrast agents, they both suffer from wide size distribution, deformed morphology, and relatively poor stability. This would in turn prejudice their chance in biomedical applications. In this regard, polymeric micelles represent a promising class of templates for the fabrication of SNCs because of their remarkable capability for nanosize and monodispersity control. Indeed, the formation of both polymeric micelles and vesicles involves a similar supramolecular self-assembly process. Nonetheless, polymeric micelles are consistently smaller than vesicles because the former comprises of only a single hydrophilic outer layer that envelops the hydrophobic interior core.

Consequently, polymeric micelles are of particular interest as soft templates for the development of SNCs because their size is normally <50 nm, which is an ideal dimension for nanocarriers to extravasate into the leaky tumour tissues and achieve passive targeting. Additionally, numerous polymeric micelles employ PEO as the hydrophilic corona, thus ensuring an excellent aqueous solubility of the micelles and stealth protection against early recognition by RES. Furthermore, the hydrophobic compartment of the polymeric micelle allows the incorporation of various functional hydrophobic compounds, such as anti-cancer drugs and imaging contrast agents. As a result, there has been increasing interest in employing polymeric micelles as structure directing agents for the fabrication of SNCs, which are aimed for the development of novel intravenous injectable nanocarriers.

There are two general approaches that have been developed for the preparation of SNCs *via* single micelle templating.[47,48] The first one involves synthesizing a designed block copolymer bearing specific functional groups. These functional groups are distributed along the corona of the polymeric micelles and serve as reservoir for the adsorption of silica precursors, thereby confining the silica condensation in the corona segment of the micelles. For example, Koh and co-workers synthesized an amphiphilic block copolymer that is terminated with silanol (Si-OH) groups at the end of the hydrophilic blocks, namely poly(methyl methacrylate)-*block*-poly(poly(ethylene glycol) methyl ether monomethacrylate)-*block*-poly(poly(ethylene glycol) methyl ether monomethacrylate-*random*-methacryloxypropyltrimethoxysilane) (PMMA-PPEGMA-poly(PEGMA-*r*-MOPS).[49] Upon the formation of polymeric micelles, the silanol groups are consequently located at the outermost region of micelles, which serve as reactive points for the formation of the silica shell, as illustrated in Figure 3. It has been shown that hybrid SNCs with particle sizes of 25 and 42 nm were synthesized respectively by tuning the molecular weight of the block copolymers.

Similarly, Yuan and co-workers synthesized cationic diblock copolymer of poly(2-(diisopropyl-amino)ethyl methacrylate)-*block*-2-(dimethylamino)ethyl methacrylate (PDPA-PDMA).[50,51] The tertiary amine groups on the PDMA block could be partially (or fully) quaternized using methyl iodide. This resulted in the formation of polymeric micelles with PDPA blocks as the hydrophobic core and the cationic PDMA blocks as the micelles corona. The cationic PDMA blocks function not only as a water solubilisation and colloidal stabilization agent, but also as a physical scaffold for silica shell growth. Interestingly, the cationic PDMA corona catalyses the hydrolysis and condensation of tetramethoxysilane (TMOS) at neutral pH and room temperature, thereby eliminating the need to employ a catalyst such as acid or base.

Khanal and co-workers designed and prepared polymeric micelles with a core/shell/corona structure from tri-block copolymers of poly(styrene-*block*-2-vinyl pyridine-*block*-ethylene oxide) (PS-PVP-PEO) after protonating the PVP blocks in a low pH (<5) environment.[52] The protonated PVP shell then acts as an acid catalyst site for the hydrolysis of silica precursor (*i.e.*, TMOS), as well as a reservoir for the adsorption of the hydrolysed TMOS *via* electrostatic interactions. The as-prepared SNCs were of 20 and 30 nm in sizes, respectively.

Specifically designed block copolymers have been well established to prepare SNCs. The approach however may incur a rather complicated organic synthesis. Therefore, single micelle templating from commercially available block copolymers is highly desired. A good candidate for such a purpose is the PEO-based block copolymers, such as the Pluronic® (PEO-PPO-PEO) family, because PEO is known to have a strong affinity to the silanol groups of hydrolysed silica precursors through hydrogen bonding. In this regard, Huo and co-workers were the first to synthesize SNCs by using single micelle templating from PEO_{106}-PPO_{70}-PEO_{106} (F127) triblock copolymers.[53] In their study, the synthesis was carried out under strong acidic condition (pH <1) so that the PEO blocks were protonated and could readily adsorb the hydrolysed silica precursors through electrostatic interactions. The highly acidic condition, together with the use of a termination agent of diethoxydimethylsilane (DEDMS) with hydrophobicity and slow hydrolysis rate, is effective on suppressing the condensation reaction between the silanol groups and thus preventing inter-particle cross-linking (*i.e.*, aggregation). As a result, the silica shell is formed surrounding the core of the F127 micelles, leaving part of the PEO blocks dangling on the as-prepared SNCs to serve as steric stabilization agent, as illustrated in Figure 4a (Route A).

Alternatively, Liu and co-workers prepared organic-inorganic hybrid SNCs by depositing an organosilane of 1,2-bis(trimethoxysilyl)ethane (BTME) onto F127 micelles in sodium phosphates (NaH_2PO_4-Na_2HPO_4) buffer solution.[48,54] This is followed by heating the polymeric

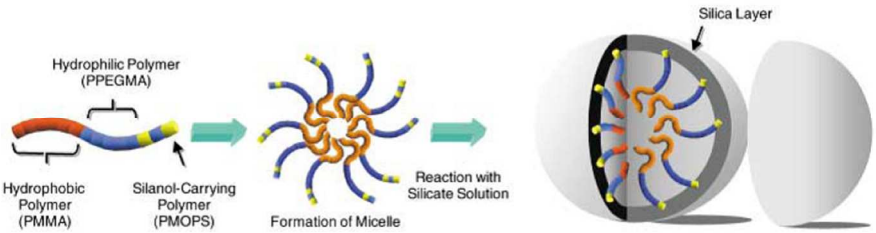

Figure 3 Schematic illustration for preparation of SNCs by using a new block copolymer functionalized with silanol groups. (Reprinted with permission from ref. 49. Copyright 2003 Wiley-VCH.)

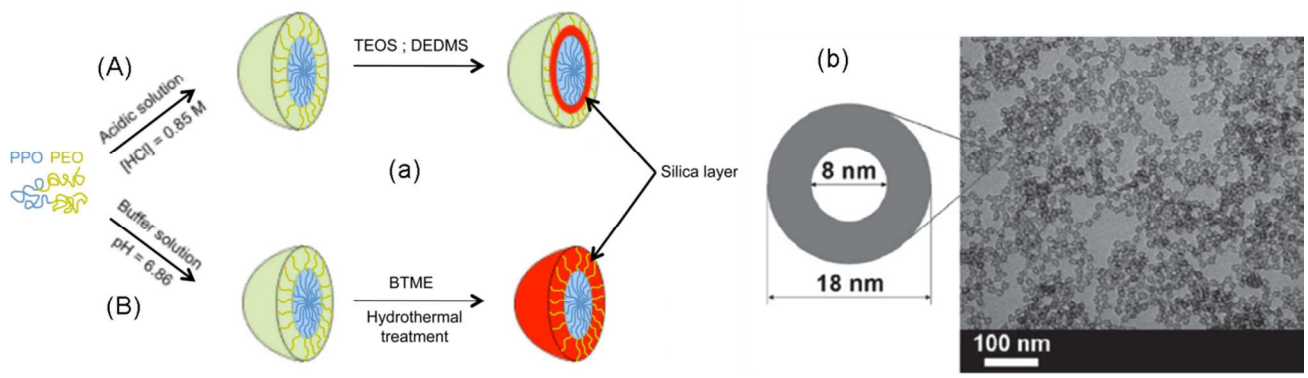

Figure 4 (a) Schematic illustration of the formation of hybrid SNCs by using F127 block copolymers as templates under strong acidic (Route A) or high temperature and pressure conditions (Route B). (b) TEM image of SNCs synthesized through Route B. (Reprinted with permission from ref. 54. Copyright 2008 American Chemical Society.)

micelles and silica precursors together in an autoclave vessel at a temperature range of 80–120 °C (Figure 4a, Route B). The as-prepared ethane-silica hybrid SNCs features microwindows (0.5–1.2 nm) in the shell, which allows for the diffusion of guest molecules into/out of the interior. In addition to the use of organosilanes to suppress the silanol cross-linking, the use of inorganic electrolytes (NaH_2PO_4-Na_2HPO_4) is also important. They are used to induce the micellization of F127 molecules at a lower concentration due to the salting-out effect. It thus generates a solution of "diluted" micelles favourable for suppression of aggregation of the micelle/silicate composites. In addition, the inorganic electrolytes can increase the ionic strength of the reaction solutions, and thus facilitate the self-assembly of the micelles and silica precursors. Other inorganic electrolytes, such as KCl, Na_2SO_4, K_2SO_4, and CH_3COONa, have also been utilized for the same purpose of avoiding aggregation.[47,48]

By contrast, the present authors' group developed an interfacial templating condensation approach to synthesize well dispersed SNCs (Figure 5).[55] The synthesis was conducted in near-neutral pH aqueous solution and at room temperature, without the use of any inorganic electrolyte or organosilane. The basic idea is to confine the hydrolysis and condensation of the silica precursors to the core/corona interface of F127 micelles so that the free dangling PEO blocks can still provide steric stabilization to the SNCs. The resultant PEOlated SNCs exhibited excellent colloidal stability both in aqueous environment and phosphate buffered solutions containing proteins (*i.e.*, antifouling property). The highly benign synthesis environment allows easy one-pot encapsulation of hydrophobic functional agents such as Fe_3O_4 nanocrystals,[56,57] MnO NPs,[58] quantum dots (QDs),[59] fluorescent conjugated polymers[60,61] and drugs,[55] providing the material with magnetic resonance imaging (MRI), fluorescence imaging, and/or drug delivery capabilities.

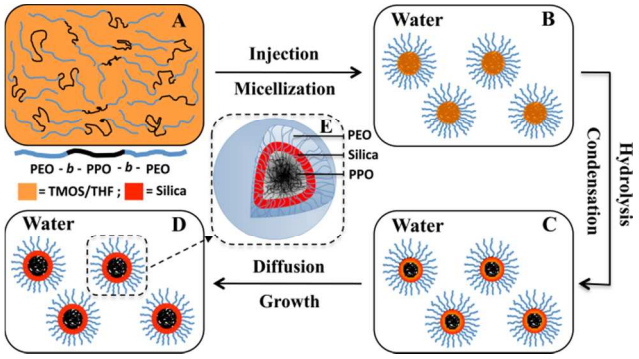

Figure 5 Schematic illustration of the formation of PEOlated SNCs through the interfacial templating condensation approach. (Reproduced from Ref. 55 with permission from The Royal Society of Chemistry.)

With the rapid development of the single micelle templating, it provides a versatile platform for the synthesis of SNCs of small size (<50 nm), high degree of uniformity, and good colloidal stability in biological fluids. The PEOlation of the as-prepared SNCs helps to further slowdown the rate of clearance by inhibiting opsonization, thereby prolonging the blood circulation half-life of SNCs.

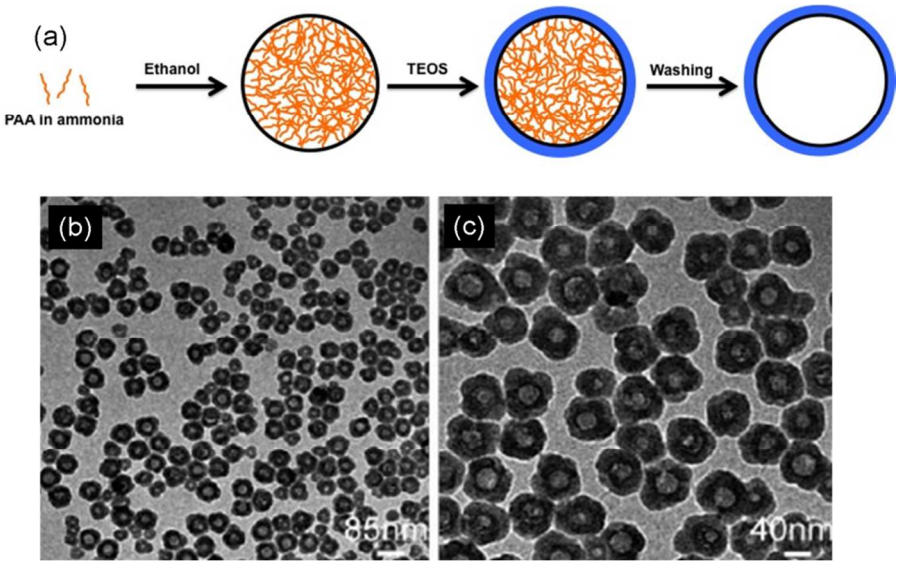

Figure 6 (a) Schematic illustration of the formation of SNCs through PAA aggregate templating. (b)–(c) TEM images of SNCs synthesized through PAA aggregate templating. (Adapted with permission from ref. 62. Copyright 2008 American Chemical Society.)

However, formation of second-order or higher-order aggregates cannot be avoided due to the cross-linking of silica. The loading capacities of SNCs are also limited by their small size. Hence, this may inevitably lead to faster drug release and less tumour-site specificity.

Polymer aggregate templating

Polymer aggregates derived from certain hydrophilic polymers such as poly(acryl acid) (PAA) and poly(vinyl pyrrolidone) (PVP) are another type of soft templates.[62–64] They are different from polymeric micelles and vesicles in that they consist of merely hydrophilic cross-linked or self-assembled polymer networks. A typical synthetic route of SNCs using PAA aggregates has been described by Yu *et al.*[62] It involves three steps (Figure 6): (1) formation of spherical PAA aggregates in a poor solvent (*i.e.*, ethanol), (2) growth of silica on the PAA aggregates; this is driven by an interaction between the aminated carboxylic groups of PAA chains and the silanol groups of hydrolysed TEOS, (3) subsequent removal of PAA by water washing. By simply adjusting the PAA concentration, this method provides a facile way to synthesize monodisperse hollow silica spheres with widely tunable diameters that ranges from 25 to 400 nm.

More complex systems such as hollow polymer aggregates are also available as soft templates. Jiang and co-workers reported the fabrication of pH-sensitive SNCs templated by hollow chitosan (CS)-PAA nanospheres,[63] as shown in Figure 7. The hollow CS-PAA templates are comprised of an outer shell of protonated and positively charged CS chains and an inner shell of CS-PAA polyelectrolyte complexes. The CS chains at the outer shell are deprotonated and act as nucleation sites for silica growth. After removing PAA by washing, CS-silica hybrid nanocapsules with double shells are achieved. The outside silica shell provides a good mechanical strength and high permeability, and the inside CS shell works as a pH-sensitive switch by swelling CS at pH = 4 and collapsing it at pH = 7.4 to open and close the pore channels in the shell, respectively. In addition, PVP aggregates are combined with dodecylamine (DDA) for the synthesis of MS-SNCs where DDA acts as a porogen in the shell.[64]

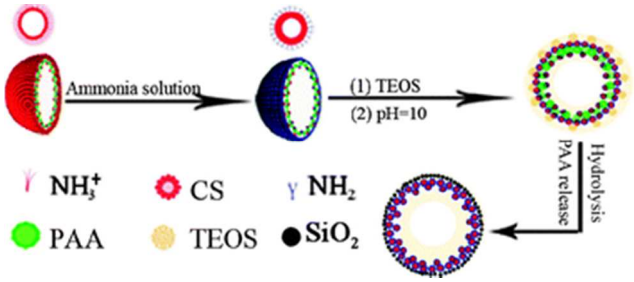

Figure 7 Schematic illustration of the formation of SNCs through hollow CS-PAA nanosphere templating. (Reproduced from Ref. 63 with permission from The Royal Society of Chemistry.)

Gas bubble templating

Another soft templating scheme for the preparation of SNCs is based on gas bubbles which can be generated from the blowing of gas or gas mixtures, *in situ* released gaseous products, or ultrasonic irradiation. Various types of gas bubbles (*e.g.*, N_2, O_2, CO_2, H_2S, PH_3, NH_3, CH_4, and air) have been applied as soft templates for the formation of hollow structures.[1] With regards to the synthesis of SNCs, a surfactant-assisted sonochemical strategy has attracted much attention due to its characteristic rapid synthesis, no requirement of any cavity-directing reagent (except for the air bubbles generated from the ultrasonic irradiation), and a facile tuning of its particle size and shell structure.

In general, the process can be conceptualized as below. The sonochemistry arises from acoustic cavitation, which is a process of continuous formation, growth, and implosive

collapse of bubbles within a liquid. Many tiny gas bubbles, which are generated from the collapse of the cavitational bubbles (~200 μm in size), serve as soft templates for the formation of hollow cavity. Surfactant molecules are enriched at the vapour-liquid interface of the tiny gas bubbles to stabilize the bubbles in a similar manner to normal liquid-liquid emulsions. They also induce a cooperative supramolecular-templated deposition of surfactant and silica surrounding the bubbles, thus leading to the formation of a mesostructured shell. The SNCs prepared *via* the gas bubble templating strategy were reported to possess wide size distributions, in the range of 50 to 500 nm.[65] The outer diameter and shell thickness of the SNCs could also be tuned by varying the sonochemical processing time, wherein more gas bubbles were available as templates with longer ultrasound irradiation time.

In summary, the quality of the soft template organization in terms of size, size distribution, stability, and proper surface affinity to silica deposition is crucial to the synthesis of SNCs. In most cases, surfactants are indispensable because they either form the soft templates directly (in vesicle and single micelle templating), or stay at the interface to stabilize the templates (in microemulsion templating). This is of paramount importance for the synthesis of nanoscale structures because the system is usually unstable due to the high surface energy. Besides, the hydrophilic segments of surfactants can also facilitate the deposition of silica through electrostatic or hydrogen interactions.

2.1.3 Template-free strategies

There are several template-free strategies developed in recent years for the preparation of SNCs. They are effective on preparing well-defined SNCs, especially rattle-type SNCs with controllable composition, size and pore structures.

Aerosol-assisted assembly strategy

The aerosol-assisted evaporation-induced self-assembly (EISA) approach was first reported by Brinker and co-workers in their work to synthesize mesoporous silica including MWHS.[1,66] Briefly, it first develops a homogeneous dilute solution containing silica precursors, volatile solvents (typically ethanol, tetrahydrofuran, HCl, and H_2O), catalysts, and surfactants. The solution is then nebulized as droplets before passing through a heated zone. Preferential evaporation of the volatile solvents causes the droplets to be enriched in silica and surfactant with radial concentration gradients. Hence, the formation of liquid-crystalline mesophase is initiated at the droplet surface and proceeds towards the droplet interior. In this way, MWHS is produced with a wide size distribution ranging from tens to hundreds of nanometers.[1,66]

In order to encapsulate functionalities into hollow silica, Tartaj and co-workers reported an aerosol pyrolysis method to incorporate γ-Fe_2O_3 into hollow silica.[1,67] In the synthesis process, functional components (*e.g.*, iron ammonium citrate) were dispersed into methanol solutions containing TEOS before nebulization. With the rapid evaporation of the methanol solvent, iron ammonium citrate and TEOS were successively precipitated and thermally decomposed at the surface of the droplet. As a result, hollow spheres of silica-coated γ-Fe_2O_3 with sizes of 50–250 nm were finally obtained. This strategy demonstrates that with the aerosol-assisted assembly approach, various moieties can be self-assembled or simply organized together within a confined droplet space. This approach is characteristic of high production rate, cost effectiveness, and adjustable dimensions from 10 nm to a few tens of micrometers. However, it suffers from broad size distributions.

Structure difference-based selective etching strategy

There is a subtle structural difference between a silica layer, which is synthesized by the Stöber method with TEOS as the single silica precursor, and that achieved by a co-condensation of TEOS and a hydrophilic organosilane (*e.g.*, aminopropyltrimethoxy silane (APTMS),[68,69] or N-[3-(trimethoxysilyl)propyl]ethylenediamine (TSD)[68,70]). As the pure silica layer has a higher degree of condensation, it is more stable against etching than the latter which is made of organic–inorganic hybrid silica. This is the basic premise of the structure difference-based selective etching strategy, which is currently gaining more attention for the preparation of SNCs. For example, Haes *et al.* reported the synthesis of three-layer sandwich structure of Au@APTMS/SiO_2@SiO_2 NPs wherein the faster ammonia etching of the middle APTMS/SiO_2 layer has resulted in the formation of Au@SiO_2 nanorattles.[68,69] Likewise, Tang *et al.* synthesized SiO_2@TSD/SiO_2@SiO_2 NPs, before using HF to selectively etch off the middle TSD/SiO_2 layer to produce SiO_2@SiO_2 nanorattles (Figure 8).[68,70]

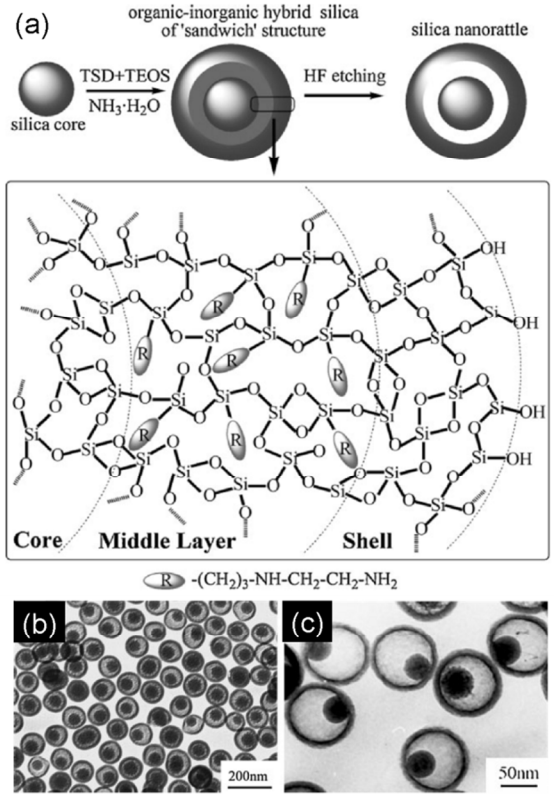

Figure 8 (a) Schematic representation of the synthesis of SiO_2@SiO_2 nanorattles through the structure difference-based selective etching strategy. (b) TEM images of silica nanorattles with different sizes and core/shell ratios. (Reprinted with permission from ref. 70. Copyright 2009 Wiley-VCH.)

Meanwhile, it was found that the hydrophobic organosilanes were able to protect the silica shell against etchant attack. Yang and co-workers reported the deposition of hydrophobic organosilanes (*e.g.*, BTME and 1,4-bis(triethoxysilyl)benzene) onto Fe_3O_4@SiO_2 core/shell NPs to form a protective layer at the external surface of the silica shell.[68,71] As a result, Fe_3O_4@SiO_2 nanorattles were successfully produced because the inner silica was dissolved more rapidly than the external layer of silica. Similarly, Shi and co-workers synthesized SiO_2@C_{18}TMS/SiO_2 core/shell NPs as templates.[68,72] In this case, C_{18}TMS is a silane coupling agent with a long hydrocarbon chain and can form hydrophobic domains within the silica shell. Consequently, it was observed that the SiO_2 core had a significantly higher density of Si-OH and therefore a lower degree of condensation than the C_{18}TMS/SiO_2 shell. This causes the inner SiO_2 core to be more prone to etching under alkaline conditions, thus favoring the formation of SNCs.

Dissolution re-deposition strategy

Lastly, a dissolution and re-deposition strategy was reported by Jang *et al.* in their synthesis of titania embedded SNCs.[73,74] Unlike the other cavity-generating strategies, this method necessitates the presence of a silica/titania interface and sonication irradiation. Consequently, silica etching is first initiated at the core/shell interface of SiO_2@TiO_2 core/shell NPs when the NPs are subjected to sonication irradiation. Next, the etched silica and sometimes titania species are dissolved into the solution and diffused out of the NPs. However, due to the Ostwald ripening process, the dissolved silica is continuously re-deposited onto the outer surface of the NPs until the hollow nanostructures is eventually formed.

2.2 Shell-forming strategies

In order to grow smooth, uniform, and robust silica layers onto cavities, an attractive interaction between the cavity templates and the silicate oligomers is required.[15] Functionalization/modification of the template surface with proper functional groups and/or electrostatic charges is sometimes necessary to ensure the compatibility between the template surface and shell material. Typically, stöber, reverse microemulsion, and supramolecular templating methods have been explored to grow silica shells. These methods are all based on a sol-gel process in which the hydrolysis of a silica precursor (*e.g.*, silicon alkoxide, organosilane or silicate) is carried out. This is followed by the polycondensation of the silanol groups to afford the desired nanocapsules. The sol-gel reactions by using a silicon alkoxide as the precursor can be described as below:

(i) hydrolysis

$$\equiv Si-OR + H_2O \rightarrow \equiv Si-OH + ROH \quad (1)$$

(ii) condensation

$$\equiv Si-OH + RO-Si \equiv \rightarrow \equiv Si-O-Si \equiv + ROH \quad (2)$$

$$\equiv Si-OH + HO-Si \equiv \rightarrow \equiv Si-O-Si \equiv + H_2O \quad (3)$$

The hydrolysis of silica precursors occurs by a nucleophilic attack of the oxygen in water molecule on the silicon atom to produce silanol groups. Hydrolysis reaction can be catalysed by adding either acid or base into the system. Once silanol groups are formed, the condensation reaction will commence to produce the siloxane bond (Si-O-Si) and by-products of alcohol (ROH) or water. Sol-gel is a popular method to form silica because the hydrolysis and condensation of silica precursors in aqueous solution can be well controlled.

Stöber and reverse microemulsion methods are two popular sol-gel methods to synthesize silica shells. The Stöber synthesis involves the hydrolysis and condensation of a silica precursor, such as TEOS, catalysed by ammonia in an ethanol/water mixture. In this method, a uniform deposition of silica from hydrolysed TEOS onto a preformed core can be easily achieved to generate the core/shell nanostructures. On the other hand, in the reverse microemulsion method, nanometer-sized water droplets are dispersed in an organic phase and stabilized by surfactants. In the synthesis of core/shell nanostructures, the core materials must enter the interior water phase followed by ammonia-catalysed hydrolysis and condensation of silica precursors at the W/O interface or in the water phase.

Supramolecular-templated deposition is another shell-forming strategy that is exclusively employed to prepare mesoporous silica shells. It typically employs a cationic surfactant (*e.g.*, CTAB) as the structure-directing agent; the strong electrostatic interaction between the positively charged surfactant molecules and the negatively charged silica ensures a cooperative deposition of the hydrolysed silica precursors, together with micelles as derived from the self-assembly of surfactant molecules, onto a preformed core. The micelles are eventually removed by pyrolysis or solvent extraction to form mesopore in the silica shell. This shell-forming strategy has been widely integrated with most of the cavity-generating strategies (as described in Section 2.1) except single-micelle templating for the preparation of MS-SNCs.

3 Structure control of silica-based nanocapsules

The structural features of SNCs and methods designed to control them have been under intensive investigation. In this section, we address their key structure features and controls over their particle sizes, level of shell porosity, cavity topology, cavity content and cargoes, and surface functionalities that are critically important for their bio-performance.

3.1 Size control

Figure 9 shows a statistic analysis of particle size and distribution of silica capsules synthesized through various synthesis methods. It clearly demonstrates the strengths and weaknesses of each method in control of size and size distribution. In general, hard templating against inorganic NPs and single micelle templating are the most effective on controlling the particle size below 100 nm and desired monodispersity. Although hard templating against polymer NPs can also generate monodisperse SNCs, it is more often used to prepare capsules larger than 100 nm in sizes. Microemulsion and emulsion (*i.e.*, macroemulsion) templating can be employed to generate silica capsules that are smaller and larger than 100 nm, respectively. However,

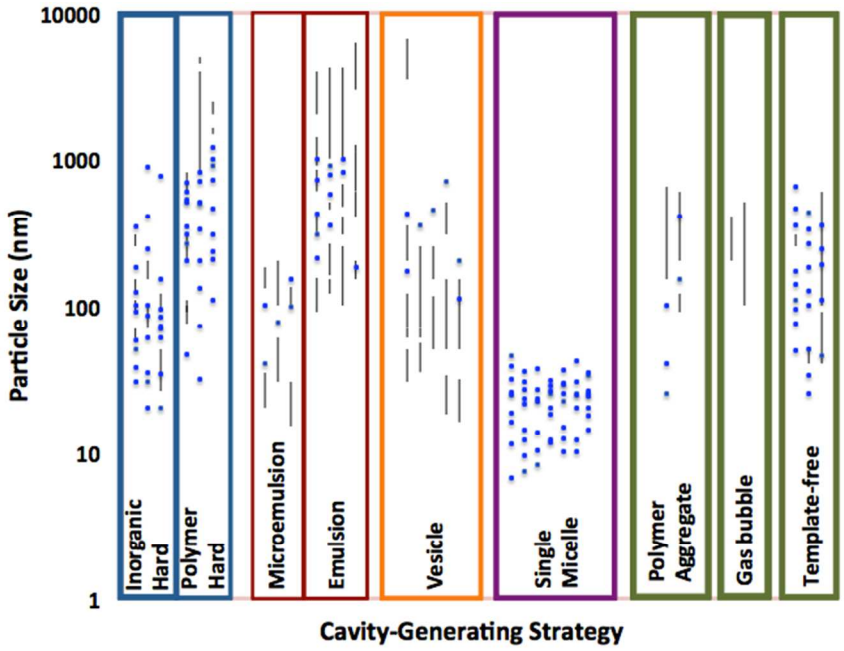

Figure 9 Particle size (up to 10 μM) and size distribution of silica capsules columned according to their synthetic strategies. The data are sourced from the publications on SNCs in 1996–2014. The size and size distributions are largely determined by TEM images.

they tend to suffer from wide size distributions. Vesicle templating is susceptible to size non-uniformity to a certain extent as it often produces capsules ranging from tens of nanometers to micrometers. In general, polymer aggregate and gas bubble methods are less commonly applied to the synthesis of SNCs. In recent years, template-free strategies have attracted increasing attention for the development of SNCs because of their good size manipulation.

Nonetheless, it should be noted that Figure 9 does not reflect the degree of particle aggregation which is otherwise significant for SNCs. This is because SNCs are very small and rich in silanol groups at the surface, thus rendering them more vulnerable to interparticle crosslinking. Such particle aggregation would hinder the use of SNCs for any application that requires a fine dispersion and function of discrete individual particles. Indeed, SNCs with small sizes and good colloidal dispersion are desirable for a prolonged blood circulation half-life. This is often a prerequisite for targeted drug delivery and sustained drug release in blood.

3.2 Porosity of silica shell

Another important attribute of SNCs is the density (or porosity) of the silica shell. This is determined by the presence of open channels/windows in the silica shell to provide pathways for the guest species to diffuse into/out of the hollow cavity. In this regard, silica-based shells can be broadly classified as purely silica shell, organic-silica hybrid shell, and supramolecular-templated mesoporous silica shell.

Silica shells prepared *via* the sol-gel chemistry approach usually exhibit an amorphous nature and possess micropores within the shells. Nann *et al.* found that the pores within the shell can be roughly estimated to be of the sub-nanometer range.[34] However, the permeability of these silica shells is not controllable, which strongly limits their applications. Hence, it is preferable to have a composite-type structure where the inorganic fraction yields mechanical strength while the organic fraction allows for controllable permeability by adjusting the hydrophobicity of shell.[53] This can be realized by the use of organosilanes that are composed of organic bridging groups.[44,45,47,48,53] A good example is the synthesis of ethane-silica SNCs through the condensation of BTME around an inorganic-electrolyte-stabilized F127 micelle under mild buffer conditions (NaH_2PO_4-Na_2HPO_4, pH ~7.0).[48,54] The PEO group can penetrate into the organosilicate layer during the assembly process, thereby resulting in the formation of micropores in the shell of SNCs. The pore size distribution based on a Horvath-Kawazoe model clearly showed the presence of micropores with a diameter in the range of 0.5–1.2 nm in the shell. Other bridging groups, such as methylene ($-CH_2-$), ethylene ($-CH_2CH_2-$), ethenylene ($-CH=CH-$), and phenylene ($-C_6H_4-$), have also been integrated in the silica framework.[47] However, the limited size scale of microwindows in organic-silica hybrid shell may still restrict certain applications, where relatively large window sizes are in demand for the adsorption and immobilization of large biomolecules.

In order to enlarge the size of pores in silica shells, a supramolecular templating strategy was developed by using surfactants as the porogen for the mesopore formation in the silica shell. In this strategy, micelles derived from the self-assembly of surfactant molecules can direct the condensation of silica precursors surrounding the micelles through electrostatic interactions or hydrogen bonding. Such mesoporous silica shells with tunable pore size, remarkable size homogeneity and high level of porosity have attractive potential in controlled release bioapplications. A large and

controllable level of porosity in the silica shell also allows to house appreciable amounts of cargoes.

3.3 Cavity topology

As described in Section 2.1.2, the cavity configuration of SNCs can be of a single compartment or an "onion"-like structure with several concentric membranes. This is largely determined by their templates of unilamellar or multilamellar vesicles, respectively. Such morphology dissimilarity affects their biomedical performance in terms of loading capacity and release rate.

In addition to the morphology variety, the cavity shape is another parameter that can be tailored. In general, SNCs take a spherical or near-spherical (probably due to the deformation of shells) shape in order to minimize the total surface free energy. The synthesis of non-spherical SNCs is much less established as compared to that of spherical SNCs. One difficulty lies in the poor availability of non-spherical templates especially for soft templates, such as micelles, vesicles and emulsion droplets, which in general prefer spherical shapes so that the interfacial energy can be minimized. Another difficulty is to deposit a uniform silica layer on surfaces with large variations in curvature.

Consequently, there have been only a few reports on the synthesis of non-spherical SNCs. In 2006, Brinker *et al.* reported the synthesis of MS-SNCs with a cubic cavity that is templated by *in situ* precipitated cubic NaCl crystals.[75] Achieved by an aerosol-assisted assembly approach (Figure 10a), the products still possessed a spherical external shape, which is largely determined by the spherical aerosol droplet. In 2008 Yu *et al.* observed the formation of an unusual ellipsoidal-shaped MS-SNCs with a silkworm cocoon-like morphology through the vesicle templating of PFOA-CTAB co-templates (Figure 10b).[43] In 2011 Wang *el al.* synthesized MS-SNCs with both a cubic-shaped cavity and cubic external shape (Figure 10c–d).[31] The synthesis strategy is based on the hard templating effect of cubic-shaped PbS NPs. In 2012, Crudden *et al.* synthesized short tube-shape SNCs through the vesicle templating of catanionic surfactants (Figure 10e).[76] Recently in 2014 Anker and co-workers achieved the synthesis of ellipsoidal MS-SNCs containing an iron nanocylinder core *via* the hard templating against hematite nanospindles (Figure 10f).[20]

Rattle-type SNCs represent another unique nanostructure in which the solid NP(s) reside in a cavity but keep an interstitial space from the silica shell. The NPs are typically made from metals or oxides that offer SNCs corresponding functionalities. A comprehensive review on the synthetic strategies for preparing rattle-type hollow structures has been done by Lou *et al*.[1] Here we will briefly focus on the strategies for the synthesis of rattle-type SNCs, as schematically illustrated in Figure 11.

Figure 11a presents a bottom-up approach: formation of NPs (*e.g.*, gold,[32] Fe_2O_3,[77] Fe_3O_4,[55–57] MnO,[58] and QDs[59]), encapsulation of single (Route I, III) or multiple NPs (Route II) in a soft material, such as microemulsion droplets, micelles and vesicles, and followed by growth of an outer silica shell.[55-59,77] The soft material-filled space or the hollow space after removing the soft material provides the nanorattles with capability to immobilize other guest molecules. Figure 11b shows another approach which also starts with the formation of NPs (*e.g.*, gold,[69] Fe_2O_3,[20] and CdSe/ZnS[34]). The NPs are then coated with a silica layer to

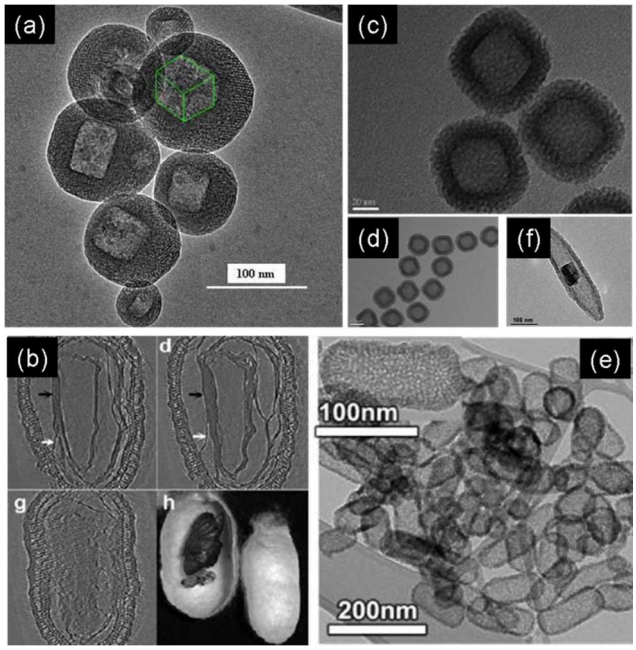

Figure 10 TEM images of non-spherical MS-SNCs. (Reprinted with permission from ref. 20,75,76. Copyright 2014, 2006 and 2012 American Chemical Society, respectively. Reproduced from Ref. 31 with permission from The Royal Society of Chemistry. Reprinted with permission from ref. 43. Copyright 2007 Wiley-VCH.)

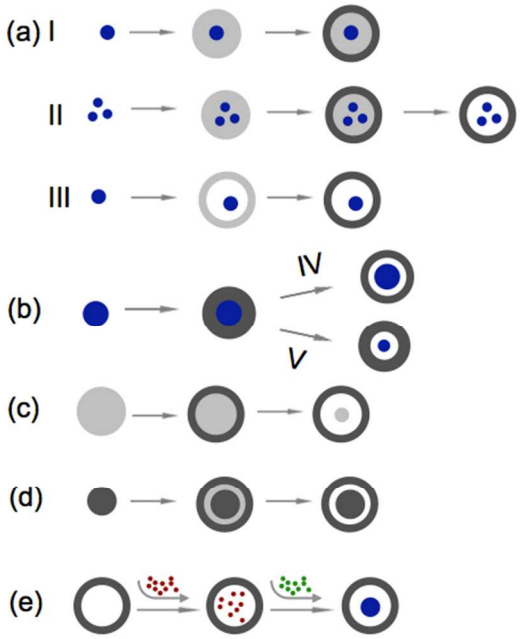

Figure 11 Schematic illustration of strategies for preparing rattle-type SNCs.

form core/shell nanostructures. The interstitial void is created by partially etching the silica shell from inside (Route IV) or the NP core (Route V).[20,34,69] Sometimes, the yolk core and shell can be made of the same materials. Figure 11c–d show two routes to form SiO_2@SiO_2 nanorattles.[35,70] Their formation involves the structure-dependent selective etching mechanism, details of which

have been described in Section 2.1.3. In addition, Figure 11e illustrates a top-down approach, in which reactants (*e.g.*, $HAuCl_4$ and $NaBH_4$[50]) are sequentially introduced to the cavity of preformed SNCs. They react inside the cavity to form a yolk (*e.g.*, Au) from within.

3.4 Cavity content and cargoes

The cavity of SNCs can be made "empty", filled with solution, or may even consist of hydrophobic polymer chains, as seen in the case of single micelle templating, wherein the templates are maintained after silica shell formation.[47,48,53,55–61,78] Interestingly, a broad variety of functional moieties have been encapsulated in the cavity of SNCs to offer bioimaging and controlled delivery capabilities. Table 2 presents an overview of the cargos that have been encapsulated in SNCs, along with their potential applications and the processes to synthesize such cargo-containing SNCs.

3.5 Surface functionalization

Extremely rich chemistry is available to functionalize the surface of SNCs, for example through co-condensation and post-synthetic grafting methods. In the one-pot co-condensation, organosilanes with functional groups are added together with the silica precursors during the synthesis of SNCs.[18,23,53,79,82,85] In this way, the functional groups are both entrapped into the silica framework and dangle on the capsule surface. In the post-synthetic grafting process, functional groups are conjugated to the exposed silica surface after the SNCs are formed.[20,24,31,73,78,80,86] This technique allows conjugation of functional groups that are not stable during the SNC synthesis. Another widely employed method in the single micelle templating synthesis is to use templates with functional groups (*e.g.*, PEO,[53,55–61] and carboxyl groups[59,60]) to functionalize the SNC surface.

To date, a large variety of functional groups have been conjugated to the SNC surface; they can be broadly classified into four types. The first type is hydrocarbon groups including methyl,[47,48,75,86] vinyl,[47] propyl,[47] phenyl,[47] octyl,[53] and other groups. They play several roles in the biomedical applications of SNCs, for example: (i) to increase the hydrophobicity of SNCs; (ii) to control the pore size of the silica shell; and (iii) to improve the particle dispersion by effectively preventing interparticle agglomeration. The second type of functional groups includes amine,[24,31,53,73,80] carboxyl,[73] sulfonate,[48] and thiol groups.[18,78,82] They are employed to tune the surface charge of SNCs and provide sites for further anchoring of other bioactive groups such as dyes and ligands. The third type of surface functional groups is bioactive molecules including fluorescein isothiocyanate (FITC),[23,79,82,86] rhodamine B isothiocyanate (RITC),[23,31,82,85] rhodamine B,[78] and folic acid.[59,60] Another important type of surface functional groups is poly(ethylene glycol) (PEG).[24,31,53,55–61,78] They form a dynamic "cloud" of hydrophilic and neutral chains over the surface of SNCs to prevent the nonspecific adsorption of proteins and enhance the long blood circulation and colloidal stability under physiological conditions.

4 Functional silica-based nanocapsules

As described in Sections 3.4 and 3.5, SNCs can be designed to intrinsical multifunction by encapsulating imaging contrast agents, drugs, or multiple agents, within the cavity, in the silica shell and/or to the nanocapsule surface, either through "one-pot" synthesis or post-treatment, therefore making them potentially useful not only in cell imaging, but also in controlled drug delivery, and targeted therapy. The following section will address the development of functional SNCs as bioimaging contrast agents, controlled drug delivery vehicles, and both.

4.1 Silica-based nanocapsules for bioimaging

SNCs have been intensively pursued for bioimaging applications by incorporation of various types of fluorescent probes (*e.g.*, organic dyes, conjugated polymers, and QDs) and magnetic nanocrystals (*e.g.*, iron oxide, and manganese oxide) because of their high colloidal and chemical stability in the physiological media, protection for photosensitive compounds with the desired image contrast (high signal-to-noise ratio), rich surface chemistry for avoiding nonspecific binding and enhancing target specificity, controllable nanoscale size with sufficiently long blood circulation, and transparency in the sense that they do not absorb much light in the near-infrared (NIR), visible, and ultraviolet regions or interfere with magnetic fields. In this section, we will briefly address the imaging capabilities of SNCs that are most commonly used for fluorescence imaging, MRI, or a combination of both modalities.

4.1.1 Fluorescent imaging

A large number of fluorescent SNCs have been developed by either encapsulating fluorescent dyes into the cavity of SNCs (Table 2) or conjugating the dye molecules to the surface of SNCs *via* chemical bonding.

Liu *et al.* reported the use of single micelle-templated SNCs for the delivery of Nile red to DU-145 human prostate cancer cells.[53] It was shown that the SNCs may not be endocytosed by the cells; instead, the dye molecules were most likely first released from the nanocapsules, permeated the cell membrane, and then stayed in the cytoplasm of cells (Figure 12a). In the work done by Yu *et al.*,[86] FITC was covalently linked to the surface of single micelle-templated SNCs through conjugation with APTMS. These FITC-labelled SNCs were evaluated by HeLa cervical cancer cells to show that surface modification of SNCs with hydrophobic methyl groups can enhance the endocytosis properties (Figure 12b). Jang *et al.* prepared various types of monodisperse titania-silica SNCs with diameters of 25, 50, 75, 100, and 125 nm and surface functional groups of amine, carboxylate, and methylene.[73] In order to systematically investigate the size- and surface functionality-dependent cellular uptake, cytotoxicity, and innate immune response of SNCs in human breast cancer (SK-BR-3) and mouse alveolar macrophage (J774A.1) cells, FITC was conjugated to SNCs. The FITC-labelled SNCs were monitored to achieve very high level of cellular uptake, cytotoxicity, and innate immune response when they are of 50 nm in size and surface functionalized with amine groups. Recently, Yu *et al.* synthesized ultrafine 10 nm-sized SNCs through the single micelle templating and demonstrated an enhanced

Table 2 A summary of cargo types, templating techniques and applications of SNCs.

Cargo type	Cargo description	Templating Strategy	Application	Ref.
Organic dye	Coumarin 153	Single micelle	Fluorescence; loading	47
	Fast green FCF, HPTSA,[a] indigo, methylene blue, oil red O, orange II, orange OT, PN[b]	Single micelle	Loading	53
	Fluorescein, Nile red	Single micelle	Fluorescence cellular imaging	53
	Hoechst 33342	PA[c]	Loading (2.01–3.3 wt%) & release	64
	Propidium iodide	PA[c]	Loading (3.22–4.82 wt%) & release	64
	Pyrene	Single micelle	Fluorescence	53
		Single micelle	Loading	47
		Single micelle	Stability against dilution test	53,55
	Sudan III	Single micelle	Loading	47,53
Fluorescent conjugated polymer	BP-PPV[d]	Single micelle	Fluorescence cellular imaging	55
	BP-PPV[d], C6PF,[e] MEH-PPV[f]	Single micelle	Fluorescence	55,57,60
	MEH-PPV[f]	Single micelle	Fluorescence cellular imaging	57,60
		Single micelle	*In vivo* fluorescence imaging	61
	PDHFBT[g]	Single micelle	Fluorescence	60
Drug	Bovine serum albumin (BSA)	Single micelle	Loading (170–585 mg/g)	48
	Cefradine	Hard	Loading & release	27
	Doxorubicin (DOX)	Hard	Loading (13.5 wt%[20] and 18.4wt%[79]) & release	20,31,79
		PA[c]	Loading (4.2–8.9%) & release; fluorescence cellular imaging	63
		Hard	*In vivo* anti-tumour growth assay	31
	Ibuprofen (IBU)	Single micelle	Loading	54
		Microemulsion	Loading (13–18 wt%) & release	80
	Indomethacin	Single micelle	Loading (8.1 wt%) & release	55
	Indomethacin, LCH,[h] procaine, vitamin B12	Single micelle	Loading	53
	L-methionine	Template-free	Loading (1.29 g/g) & release	81
	Nabumetone, naproxen, papaverine	Single micelle	Loading & release	53
Inorganic NP	Au	Hard	Plasmon resonance	32
		Template-free	Surface-enhanced Raman scattering	69
		Vesicle		77
		Single micelle		50
	Fe	Hard	T2-weighted MRI, $r_2 = 284.7$	20
	Fe_2O_3	Vesicle		77
	Fe_3O_4	Microemulsion	T2-weighted MRI	35
		Single micelle	T2-weighted MRI, $r_2 = 228$,[56] 127.8,[57] 215.3,[78] and 10.6–176.1 $mM^{-1}s^{-1}$ [82]	56,57,78,82
		Single micelle	*In vivo* MRI	78
		Template-free	Superparamagnetism	71
	MnO	Single micelle	T1-weighted MRI, $r_1 = 1.17$ $mM^{-1}s^{-1}$	58
	MnO (hollow)	Hard	T1-weighted MRI, $r_1 = 0.14–0.2$[83] and 0.99 $mM^{-1}s^{-1}$ [84]	83,84
		Hard	*In vivo* MRI	84
	Gd-DTPA[i]	Hard	T1-weighted MRI, $r_1 = 8.6$ $mM^{-1}s^{-1}$	20
	CdSe/CdS/ZnS	Single micelle	Fluorescence cellular imaging	59
	CdSe/ZnS	Microemulsion	Fluorescence	80

[a] HPTSA: 8-Hydroxypyrene-1,3,6-trisulfonic acid; [b] PN: N-phenyl-1-naphthylamine; [c] PA: polymer aggregate; [d] BP-PPV: poly{2-[2'-phenyl-4',5'-di(3"-methyl-butoxy)phenyl-1,4-phenylenevinylene]}; [e] C6PF: poly(9,9-dihexylfluorenyl-2,7-diyl); [f] MEH-PPV: poly[2-methoxy-5-(2-ethyl-hexyloxy)-1,4-phenylenevinylene]; [g] PDHFBT: poly(9,9-dihexylfluorenyl-2,7'-diylbithiophene); [h] LCH: lidocaine hydrochloride; [i] Gd-DTPA: diethylenetriaminepentaacetic acid gadolinium(III) dihydrogen salt hydrate.

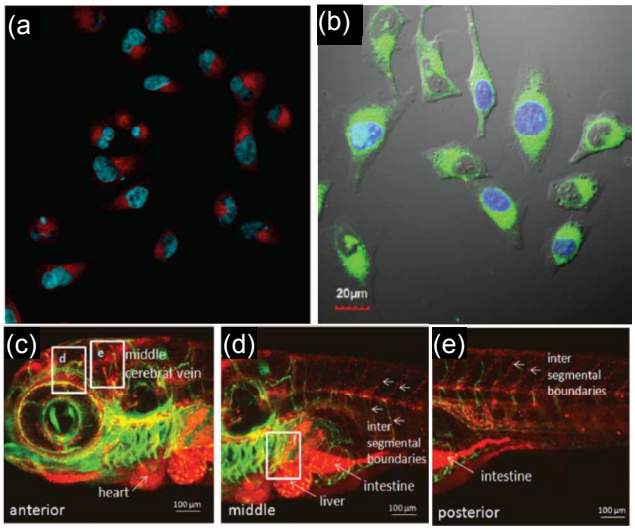

Figure 12 (a) Confocal fluorescence image of DU-145 human prostate cancer cells cultured with Nile red-labelled SNCs, showing red contrast inside the cell but outside the cell nuclei (stained in blue). The cell size ranges from 3 to 5 μm. (b) Merged fluorescence and bright-field image of HeLa cells cultured with FITC-labelled SNCs, showing green contrast can even penetrate the membrane of the nucleus. (c)–(e) Confocal images of transgenic zebrafish larvae, illustrating the biodistribution and uptake of MEH-PPV-labelled SNCs (as indicated by red contrast) after 1 day post injection into the heart. (Reprinted with permission from ref. 53. Copyright 2006 American Chemical Society. Reproduced from Ref. 61,86 with permission from The Royal Society of Chemistry.)

penetration ability of RITC-labelled SNCs in U87MG glioma spheroids, a three-dimensional solid tumour, as compared to that of conventional mesoporous silica NPs.[85]

In addition to the most commonly used organic dyes, fluorescent conjugated polymers have recently emerged as an alternatively promising class of fluorescent probes in cellular imaging. This is because they exhibit rather stable and bright emission, high level of photostability, low degree of toxicity and wide wavelength versatility. The present authors' group has reported the preparation of fluorescent SNCs by encapsulating fluorescent conjugated polymer through the single micelle templating method.[60] Four different fluorescent conjugated polymers, namely C6PF, BP-PPV, PDHFBT, and MEH-PPV, which emit blue, green, yellow, and red colours, respectively, were encapsulated in the SNCs. The *in vitro* studies by using BV-2 microglial cells and MDA-MB-231 breast cancer cells showed that the conjugated polymer-labelled SNCs were uptaken and located at the cytoplasm of the cells.[55,60] The MEH-PPV-labelled SNCs were further studied *in vivo* with transgenic zebrafish line TG(fli1:EGFP) as the vertebrate model.[61] The biodistribution of fluorescent SNCs, which was examined in the whole larvae, 1-day post injection (Figure 12c–e), clearly showed that the red contrast of MEH-PPV-labelled SNCs was predominantly detected close to the green fluorescent (GFP-positive) blood vessels. *In vivo* biocompatibility was also affirmed as the cellular internalization of these fluorescent SNCs did not interfere with larval development nor affect vessel growth. Their biostability was verified by the presence of fluorescent-labelled cells even after 7 days since the initial exposure to the microinjected silica nanocarriers.

Alternatively, the present authors' group has recently encapsulated CdSe/CdS/ZnS QDs into single micelle-templated SNCs.[59] The surface of SNCs was further conjugated with folate for target specificity. *In vitro* testing using MDA-MB-231 cells with overexpression of folate receptors demonstrated the efficacy of a targeted delivery of QDs to the cancer cells.

4.1.2 Magnetic resonance imaging

MRI contrast arises from the relaxation of water protons when subjected to the influence of an external magnetic field and a radio-frequency (RF) pulse. There are two different relaxation pathways: longitudinal (T1) and transverse (T2) relaxations. In this regard, MRI contrast agents are substances that could be used to reduce the T1 or T2 of the water protons, thereby increasing the signal difference between the area of interest and the background. There are two main classes of MRI contrast agents: paramagnetic Mn(II), Mn(III), or Gd(III)-containing contrast agents, and superparamagnetic iron oxide (SPIO) contrast agents.

T1 magnetic resonance imaging

In recent years, the use of SNCs to encapsulate MRI T1 contrast agents (*e.g.*, MnO NPs) has been demonstrated to enhance the ability of these "positive" contrast agents to exert a more hyperintense region and thus a higher r_1 relaxivity. Silica itself has been recognized as a good candidate to coat T1 contrast agents because it is bio-inert and generally non-toxic. Coupled with the desired mechanical stability of silica, it ensures that the integrity of the nanocarrier can be maintained during the delivery of its payload in the bloodstream. Yet, it has been argued that the traditional MnO@SiO_2 core/shell NPs may have a detrimental effect on the r_1 relaxivity of the contrast agent. This is because a dense, non-porous silica coating, which is typically synthesized *via* the conventional Stöber method or the reverse microemulsion technique, can hinder the interactions between water molecules and the MnO NPs, thereby diminishing the r_1 relaxivity. In this regard, adopting a nanocapsule structure has been demonstrated to be able to overcome some of these drawbacks that are associated with the core/shell morphology.

Single micelle-templated SNCs have been used to improve the water dispersibility, biocompatibility, and r_1 relaxivity of MnO NPs. For example, the present authors' group has designed a hybrid coating to encapsulate MnO NPs.[58] The coating layer that consists of a thin and porosified silica shell perforated by the PEO chains of F127 can allow for the rapid penetration of water molecules to the encapsulated MnO core. In addition, these SNCs exhibited a nanorattle structure, wherein the "empty" space surrounding the MnO core was believed to benefit the MRI T1 performance by facilitating the passage of water molecules to the surface Mn ions. The consequent enhancement of T1 contrast was further confirmed with a pre-clinical 7 T MRI scanner, wherein an r_1 relaxivity of 1.17 $mM^{-1}s^{-1}$ was measured when 15 nm-sized MnO NPs were encapsulated. This is indeed better than the r_1 values reported for other 15 nm-sized MnO NPs that are encapsulated with commonly used

surface coatings such as PEG-phospholipid or non-porous silica.

As a shell coating for MnO NPs, the use of mesoporous silica will also improve the accessibility of water molecules to the MnO core significantly due to the presence of mesopores in the silica shell. Hence, the water proton relaxation rate can be greatly increased by a close proximity of the water molecules to Mn^{2+} ions on the surface of MnO core. Moreover, by etching the MnO NPs with an acid solution or *via* the Kirkendall effect, a hollow MnO core can be produced for a higher surface-to-volume ratio. The higher Mn^{2+} concentration at the hollow inner surface will result in a higher r_1 relaxivity of MnO NPs. Such effectiveness has been clearly demonstrated by several research groups.[83,84] A key feature of these SNCs with a mesoporous shell and a hollow MnO core is that their interior surface still retains a thin MnO layer even after the nanoscale etching process.

T2 magnetic resonance imaging

Development of T2 MRI contrast agents has been extensively studied and iron oxide nanocrystals with high value of magnetization and a narrow size distribution are found to be excellent T2 MRI contrast agents. However, the application of iron oxide nanocrystals requires an appropriate coating on the surface to make them nontoxic and biocompatible. In this regard, SNCs endow the magnetic nanocrystals not only good biocompatibility but also enhanced chemical and mechanical stability. The present authors' group has reported the fabrication of PEOlated SNCs with the encapsulation of hydrophobic Fe_3O_4 nanocrystal clusters.[56] The products thus developed exhibited a high saturation magnetization (15.21 emu/g). The T2-weighted properties were measured with a 1.5 T scanner. The r_1 and r_2 relaxivity values were reported to be 6.9 and 228 $mM^{-1}s^{-1}$, respectively. The relaxivity ratio, r_2/r_1, was calculated to be 33; this is much higher than ferucarbotran (~19) and other dextran-coated SPION (3–19).

4.1.3 Multimodal imaging

SNCs have also been extensively explored for multiple imaging modalities, such as a combination of fluorescence and MR imaging. One of the main objectives here is to produce a multifunctional tool that is able to perform different tasks simultaneously. Mou *et al.* reported the preparation of Fe_3O_4/FITC@SNCs through the reverse microemulsion templating, wherein FITC was bonded to the silica shell through the use of organoalkoxysilane derivatives.[35] It was observed that 90% of the products possessed a single Fe_3O_4 core. The bi-functional SNCs were successfully internalized into many different cells such as HeLa, MCF-7 and NIH3T3, as evidenced by the confocal fluorescence images. They also displayed a distinct contrast in the *in vitro* T2-weighted MR image.

Shi and co-workers have successfully synthesized another type of bi-functional SNCs through the single micelle templating.[78] Each SNC consists of multiple superparamagnetic nanocrystal cores, a rhodamine B-doped silica shell, polymeric micelle of poly(ε-caprolactone)$_{100}$-*block*-poly (acrylic acid)$_{35}$, and PEG chains grafted onto the particle surface (PEGylated Fe_3O_4/dye@SNCs). T2-weighted MRI properties were measured with a 3 T scanner and the calculated r_2 relaxivity value was 215.3 $s^{-1}mM^{-1}$, which is higher than the non-clustered magnetite NP system. In view of the low cytotoxicity and excellent colloidal stability, the potential application of PEGylated Fe_3O_4/dye@SNCs as T2 contrast agents was further evaluated *in vivo*. For example, *in vivo* test was performed by injecting PEGylated Fe_3O_4/dye@SNCs into tumour-bearing mice. After 40 minutes post-injection, significant accumulation of the SNCs was detected in the tumour area with a T2 signal intensity drop of 42% (Figure 13). Thus, the passive targeting of PEGylated Fe_3O_4/dye@SNCs *via* the enhanced permeability and retention (EPR) effect was demonstrated. The accumulation was further confirmed by *ex vivo* Prussian blue staining of the tumour tissue from the sacrificed mouse at 5 hour post-injection.

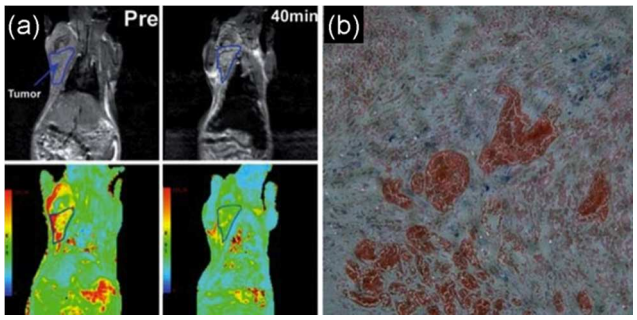

Figure 13 (a) *In vivo* T2-weighted MR images (upper) and colour mapped images (lower) of a tumour site before and 40 minutes after intravenous injection of PEGylated Fe_3O_4/dye@SNCs (the marked regions indicate tumour site); (b) *Ex vivo* Prussian blue staining images of tumour tissues which were selected from mice at 5 h post-injection of PEGylated Fe_3O_4/dye@SNCs. (Reproduced from Ref. 78 with permission from The Royal Society of Chemistry.)

Furthermore, the delivery of multifunctional SNCs in a targeted manner has been investigated by applying an external magnetic field.[57] In the study, PEOlated Fe_3O_4/MEH-PPV@SNCs, which were synthesized *via* the single micelle templating approach, consist of the conjugated polymer MEH-PPV as the fluorescent emitter and SPIONs as the magnetic constituent, both of which are encapsulated inside the cavity of SNCs. The *in vitro* studies showed that the multifunctional SNCs can be guided to the HepG2 cancer cells by simply applying an external magnetic field. Therefore they demonstrate great potential for magnetic targeting biomedical applications (Figure 14).

MS-SNCs have been commonly used for dual MR and optical imaging applications. This is due to the good accessibility of water molecules through the mesoporous silica shell, thereby enabling them to increase the r_1 relaxivity of encapsulated T1 MR contrast agents. Besides, the mesoporous silica shell can also be readily functionalized with various organic dyes for fluorescence imaging capabilities. In this regard, Chou *et al.* designed a bifunctional nanocomposite that is composed of a single hollow MnO NP encapsulated within an iridium (Ir)-functionalized mesoporous silica shell.[83] Its versatility as a dual imaging probe was demonstrated because the Ir complex could yield a strong red phosphorescence even under *in vitro* conditions while the hollow magnetic core is responsible for the signal enhancement on T1-weighted MR images *in vitro*. Similarly, Hyeon and co-workers synthesized mesoporous silica-coated hollow manganese

oxide NPs, with the fluorescent organic dye, RITC, conjugated to the silica surface using simple silane conjugation chemistry. Intracranial grafting of these nanoparticles enabled serial MR monitoring of cell transplants over a prolonged time period. Moreover, they could also be readily uptaken by adipose-derived mesenchymal stem cells for cell labelling and cellular imaging *in vitro*.

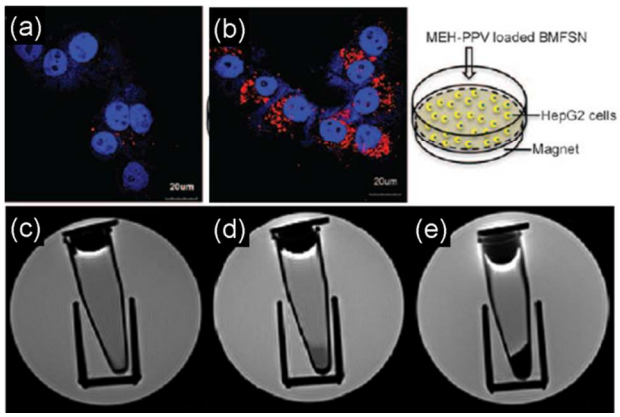

Figure 14 Confocal fluorescence images of HepG2 cells cultured with 120 μg/mL of PEOlated Fe_3O_4/MEH-PPV@SNCs without (a) and with (b) influence of an external magnetic field, showing a marked increase in the red emission of the cells cultured upon the application of an external magnetic field. (c)–(e) T2-weighted MR images of the HepG2 cells were acquired by using a spin-echo pulse sequence in a 7 T MR scanner: (c) control, (d) and (e) were incubated with 60 μg/mL of PEOlated Fe_3O_4/MEH-PPV@SNCs without and with the presence of an external magnetic field, respectively. A darker MR contrast was observed for the cells treated with the magnetic field relative to that of the cells cultured without the field. (Reprinted with permission from ref. 57. Copyright 2011 American Chemical Society.)

4.2 Silica-based nanocapsules for drug delivery

Over the past couple of decades, cancer nanotherapeutics have rapidly progressed and many types of nanoscale drug carriers, such as liposomes, polymers (*e.g.*, micelles, dendrimer, and polygels), and inorganic NPs (*e.g.*, mesoporous silica, and metallic NPs) have been developed, and some are now even available in the market. Within this context, the development of SNCs as controlled drug delivery vehicles has attracted much attention. They have been widely used to solubilize and carry drugs that exhibit relatively poor solubility, low stability, or undesirable pharmaceutical properties. Their small sizes and excellent colloidal and chemical stability allow them to circulate in the body for a long period of time. Hence, they are able to penetrate the leaky vasculature of tumours and accumulate in the affected area more easily.

A range of drugs, both hydrophilic and hydrophobic, have been explored for encapsulation in SNCs. The most typical way is to soak SNCs in a drug solution so that the drug molecules are diffused into the SNC cavity.[54,79] Alternatively, the drugs can also be facilely encapsulated in SNCs *via* a one-pot synthesis step.[47] Specific drugs such as L-methionine were encapsulated within the spherical cavity at a high level of loading by repeated crystallization.[81] However, the nanoscale size of SNCs can limit their physical space for drug encapsulation. Moreover, the use of SNCs (especially MS-SNCs) as drug carriers is susceptible to a rapid and near burst drug release from the nanostructure.[27] Brinker *et al.* observed that L-methionine was released within 3 minutes in phosphate buffered saline because of the high aqueous solubility of the drug and fast diffusion rate of the small L-methionine molecules through mesoporous silica shell.[81]

To accomplish a better storage and sustained release of drugs, the pore openings in the silica shell of SNCs and the interactions between drugs and SNCs have to be manipulated, mostly through the surface modification of the SNCs. It was reported that the release rate of DOX from the PEG-modified SNCs was significantly slowed down due to the reduced pore size by conjugating PEG molecules on the small pore walls.[24] As a result, the sample exhibited near zero-order kinetics without initial burst release. It was also reported that the CH_3-modified SNCs exhibited a decrease in pore size from 2.06 to 1.50 nm due to the occlusion of the pore channels with methyl groups.[75] This greatly slowed down the release of NaCl (although it is not a drug) from several seconds to 80 hours. In addition, two types of interactions between drugs and SNCs, namely the electrostatic interaction and the hydrophobic interaction, have been explored to tune the loading capacity and release rate of SNCs. As has been reported, NH_2-modified SNCs exhibited a higher loading capacity and a slower release rate of the drug of naproxen as compared to the unmodified SNCs. This is attributed to the electrostatic interaction between the carboxyl group of naproxen and the amino group of SNCs.[53] Similarly, other carboxyl group-containing drugs (*e.g.*, DOX and ibuprofen) have been shown to exhibit a decreased release rate when encapsulated by the NH_2-modified SNCs.[24,80] Alternatively, increasing the condensation degree of silica or introducing organic groups to the silica matrix could increase the hydrophobicity of silica. As a result, there is a stronger hydrophobic interaction between the drugs and SNCs, thereby leading to a higher level of drug loading and a slower release rate.[53] Yang *et al.* reported a shell-thickness-dependent drug release behaviour in MS-SNCs. The release amount and release rate of DOX were increased by a decrease in the shell thickness.[79]

In addition, the release behaviour can be controlled precisely by pH-responsive nanovalves.[64] The concept is schematically illustrated in Figure 15. Herein, the MS-SNCs contained anilinoalkane stalks (covalently bonded to the silica surface) and bulky nanovalves of α-CD (a cyclic molecule which encircles the stalks *via* non-covalent interactions). When pH of the environment is changed, the bulky cyclic groups of α-CD will block or unblock the pores on the surface of MS-SNCs, respectively. For example, at pH ~7, the α-CD rings are complexed with the stalks; this causes the bulky cyclic components to block the pores. Upon decreasing the pH environment, which occurs in several physiological and pathological processes such as endosome trafficking, tumour growth, inflammation, and myocardial ischemia, the aniline nitrogens on the stalks are protonated. This lowers the binding affinity between α-CD and the stalks, thereby causing the α-CD to dissociate, unblock the pores and then release the encapsulated cargo molecules from the interior.

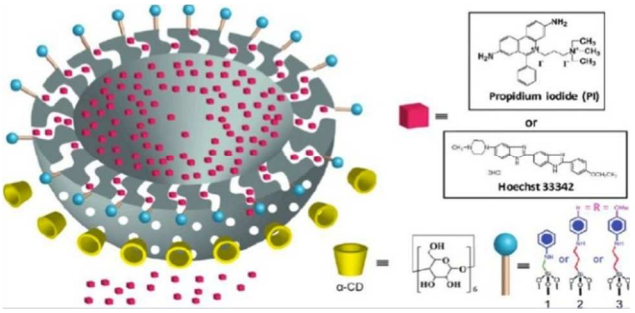

Figure 15 Schematic illustration of a cross section of MS-SNC showing the wormlike pores connecting the interior to the surrounding medium. The stalks and the α-CD rings that control the pore openings are also shown. (Reprinted with permission from ref. 64. Copyright 2009 American Chemical Society.)

4.3 Silica-based nanocapsules for nanotheranostics

Based on the functionalities briefly described above, SNCs represent an excellent scaffold for the facile loading of a wide variety of bioimaging and therapeutic moieties. As such, they are promising candidates for nanotheranostics for simultaneous imaging and therapy applications. This integrated system holds great promises because it could monitor the real time drug release and distribution, thus predicts and validates the efficacy of the treatment.

To improve the performance of nanotheranostics, surface of SNCs is modified by tethering protective ligands, such as PEG,[24,31,53,55–61,78] to prolong the bioavailability of the nanotheranostics. Other modifications include conjugating targeting ligands, such as folic acid,[59,60] to the SNC surface to trigger receptor-mediated endocytosis, thereby enhancing the biodistribution and uptake of the nanotheranostics in the targeting area. In addition, SNCs must retain their drug payload with "zero leakage" throughout the long circulation period before reaching the targeting site. The integrated system could then undergo a stimuli-responsive release of drugs at a satisfactory rate to ensure its bioavailability and pharmacological activity.

For example, Jiang and co-workers reported the use of CS-silica double shelled nanocapsules to load the anti-cancer drug of DOX for pH-sensitive nanotheranostics.[63] The inner CS shell served as a pH-sensitive switch. Under the "off" status at pH = 7.4, CS was deprotonated and collapsed at the pore openings to restrict the release of DOX. Under the "on" status at pH = 4, the amino groups in CS were protonated. This caused the positively charged CS to swell and expose the pore openings so that the drug was released. Therefore, the release profile exhibited a pulse appearance while the drug release could be switched on and off by alternately changing the medium pH value (Figure 16b). Figure 16c showed the fluorescence image of DOX-loaded CS-silica nanocapsules incubated with LoVo cells as obtained in the green channel. It clearly showed that most of the DOX was inside the cells and even in the nucleus. The DOX-loaded CS-silica nanocapsules showed better cellular uptake than free DOX, probably due to the endocytosis mechanism, and thus a higher level of therapeutic efficiency (Figure 16d).

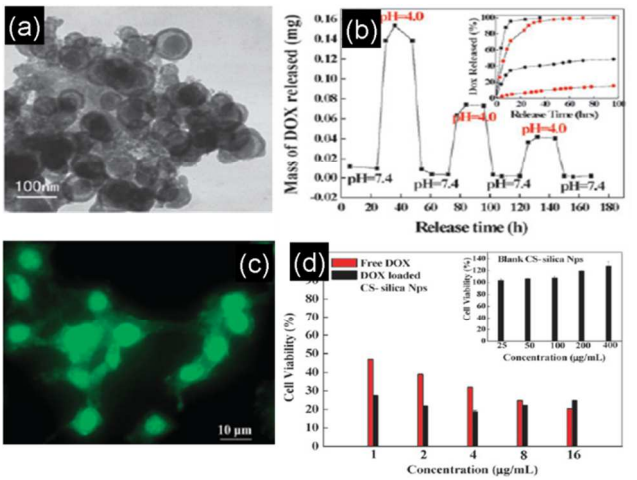

Figure 16 (a) TEM images of CS-silica double-shelled nanocapsules. (b) *In vitro* release profile of DOX-loaded CS-silica nanocapsules at 37 ^{o}C with pH values of the release medium alternately changed between 7.4 and 4.0. (c) Fluorescence image of DOX-loaded CS-silica nanocapsules incubated with LoVo cells for 4 hours. (d) *In vitro* cytotoxicity of free DOX and DOX-loaded CS-silica nanocapsules against LoVo cells. Inset is the cytotoxicity of empty CS-silica nanocapsules against LoVo cells. (Reproduced from Ref. 63 with permission from The Royal Society of Chemistry.)

In another study,[31] multifunctional PEGylated MS-SNCs, which were labelled with RITC for fluorescence behaviour, were able to release DOX in tumour-bearing mice to demonstrate a more effective tumour growth inhibition efficacy (39.10%) than free DOX (22.33%).

Anker and co-workers recently reported a rattle-type SNC which can function as a dual MRI contrast agent, as well as a pH-responsive drug delivery system.[20] The Fe/DOX/Gd-DTPA@SNC@AL/PLL NPs consist of an iron NP and an ellipsoidal silica shell that is loaded with DOX and the T1 contrast agent Gd-DTPA (Figure 17). The surface of the ellipsoidal nanotheranostics was decorated with biocompatible poly-L-lysine (PLL) and sodium alginate (AL) to control the DOX release. The products thus derived demonstrated a very high saturation magnetization of 63.4 emu/g. The T1-weighted and T2-weighted properties were studied with a 4.7 T MRI instrument. The r_1 was measured as 8.6 $mM^{-1}s^{-1}$, which is higher than that of the free Gd-DTPA and the r_2 was measured as 285 $mM^{-1}s^{-1}$, which is much higher than that of the FDA-approved iron oxide NP contrast agents. Furthermore, DOX was loaded into the cavity of the nanocapsules for controlled drug release. It was observed that the release of DOX was highly pH-sensitive as its release rate was significantly increased under acidic conditions. Cellular therapeutic efficiency, which was studied using MCF-7 breast cancer cells, also indicated that the NPs exhibited a higher cytotoxicity than free DOX.

The loading of SNCs with phthalocyanine photosensitizers has also been recently reported. Carriers of these therapeutic molecules were able to kill cancer cells (both *in vitro* and *in vivo*) by a combined photodynamic and photothermal effect.[87]

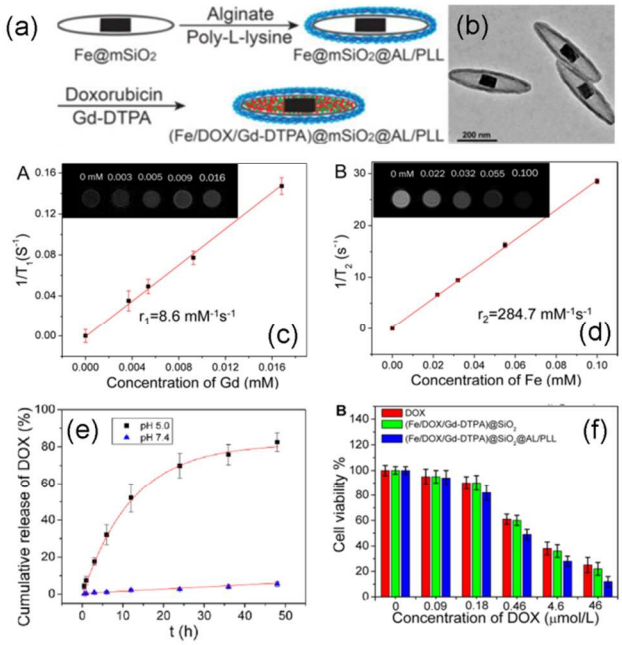

Figure 17 (a) Schematic illustration showing the synthesis route of Fe/DOX/Gd-DTPA@SiO_2@AL/PLL. (b) TEM image of Fe@SNC@AL/PLL. (c) T1 and (d) T2-weighted images of magnetic at echo time of 4 ms. (e) pH-triggered release profile of DOX from Fe/DOX/Gd-DTPA)@SNC@AL/PLL. (f) Cell viability of MCF-7 cells after incubating with different drug formulations at different concentrations for 48 h. (Reprinted with permission from ref. 20. Copyright 2014 American Chemical Society.)

5 Conclusions and outlook

There has been intensive progress in syntheses, structure controls, surface functionalization, and biomedical applications of SNCs, as described in this review. SNCs are promising platforms that can be engineered with varying structural configurations and numerous multifunctionalities for biomedical imaging and theranostic applications. Several synthetic strategies have been developed for SNCs, with varying degrees of success in terms of structure control and surface functionalization. Both *in vitro* and *in vivo* studies have demonstrated their potential as diagnostic and therapeutic agents. However, several areas still require considerable study before SNCs are fully established for the proposed applications. For example, SNCs are expected to be functionalized with more specific types of targeting ligands and be designed more precisely responsive to the applied stimuli so that the cellular uptake and delivery process is more targetable and controllable. SNCs are also promising for gene therapy by conjugating gene binder such as nucleic acids to their outer surfaces. The *in vivo* biocompatibility, biodistribution, targeting efficiency, toxicity, biodegradability and clearance of SNCs also need to be further studied. The research focuses in this field will include design and synthesis of "smart" multifunctional SNC nanocarriers, *in vivo* performance evaluation using animal models and subsequent translational studies. Therefore, multi-disciplinary collaborations are critical among materials scientists, chemists and clinicians to enable the utilization of SNCs in clinics. Apart from the biomedical applications, SNCs also provide a unique platform for encapsulation of functional agents for heterogeneous catalysis, separation, optoelectronics, magnetic resonance and chemical sensing applications. They can serve as the solid templates for growth of various novel nanostructures. The synthetic strategies developed for SNCs can be extended to other organic and/or inorganic capsules.

Notes and references

[a] Department of Materials Science & Engineering, National University of Singapore, Singapore.
[b] NUS Graduate School for Integrative Sciences and Engineering, National University of Singapore, Singapore.
[c] Institute of Materials Research and Engineering, Agency for Science, Technology and Research (A*STAR), 3 Research Link, Singapore.
Email: msewangj@nus.edu.sg; x-li@imre.a-star.edu.sg

1 X. W. Lou, L. A. Archer and Z. Yang, *Adv. Mater*, 2008, **20**, 3987–4019.
2 Y. Zhao and L. Jiang, *Adv. Mater*, 2009, **21**, 3621–3638.
3 J. Hu, M. Chen, X. Fang and L Wu, *Chem. Soc. Rev.*, 2011, **40**, 5472–5491.
4 L. L. Zhang and X. S. Zhao, *Chem. Soc. Rev.*, 2009, **38**, 2520–2531.
5 M. Antonietti and S. Förster, *Adv. Mater*, 2003, **15**, 1323–1333.
6 H. J. Fan, U. Gösele and M. Zacharias, *Small*, 2007, **3**, 1660–1671.
7 V. Sokolova and M. Epple, *Angew. Chem. In. Ed.*, 2008, **47**, 1382–1395.
8 Z. Li, J. C. Barnes, A. Bosoy, J. F. Stoddart and J. I. Zink, *Chem. Soc. Rev.*, 2012, **41**, 2590–2605.
9 P. T. Tanev and T. J. Pinnavaia, *Science*, 1996, **271**, 1268–1269.
10 S. Schacht, Q. Huo, I. G. Voigt-Martin, G. D. Study and F. Schüth, *Science*, 1996, **273**, 768–771.
11 F. Caruso, R. A. Caruso and H, Möhwald, *Science*, 1998, **282**, 1111–1114.
12 S. S. Kim, W. Zhang and T. J. Pinnavaia, *Science*, 1998, **282**, 1302–1305.
13 J. L. Vivero-Escoto, R. C. Huxford-Phillips and W. Lin, *Chem. Soc. Rev.*, 2012, **41**, 2673–2685.
14 A. Burns, H. Ow and U. Wiesner, *Chem. Soc. Rev.*, 2006, **35**, 1028–1042.
15 J. J. L. M. Cornelissen, E. F. Connor, H.-C. Kim, V. Y. Lee, T. Magibitang, P. M. Rice, W. Volksen, L. K. Sundberg and R. D. Miller, *Chem. Commun.*, 2003, 1010–1011.
16 J. Yang, J. U. Lind and W. C. Trogler, *Chem. Mater.*, 2008, **20**, 2875–2877.
17 H. Blas, M. Save, P. Pasetto, C. Boissière, C. Sanchez and B. Charleux, *Langmuir*, 2008, **24**, 13132–13137.
18 J. Yuan, D. Wan and Z. Yang, *J. Phys. Chem. C*, 2008, **112**, 17156–17160.
19 N. Kato, T. Ishii and S. Koumoto, *Langmuir*, 2010, **26**, 14334–14344.

20 H. Chen, D. Sulejmanovic, T. Moore, D. C. Colvin, B. Qi, O. T. Mefford, J. C. Gore, F. Alexis, S. -J. Hwu and J. N. Anker, *Chem. Mater.*, 2014, **26**, 2105–2112.
21 D. K. Yi, S. S. Lee, G. C. Papaefthymiou and J. Y. Ying, *Chem. Mater.*, 2006, **18**, 614–619.
22 W. Zhao, M. Lang, Y. Li, L. Li and J. Shi, *J. Mater. Chem.*, 2009, **19**, 2778–2783.
23 J. Kim, H. S. Kim, N. Lee, T. Kim, H. Kim, T. Yu, I. C. Song, W. K. Moon and T. Hyeon, *Angew. Chem. Int. Ed.*, 2008, **47**, 8438–8441.
24 J. Yang, J. Lee, J. Kang, K. Lee, J. -S. Suh, H. -G. Yoon, Y. -M. Huh and S. Haam, *Langmuir*, 2008, **24**, 3417–3421.
25 Z. -Z. Li, L. -X. Wen, L. Shao and J. -F. Chen, *J. Controlled release*, 2004, **98**, 245–254.
26 J. -F. Chen, J. -X. Wang, R. -J. Liu, L. Shao and L. -X. Wen, *Inorg. Chem. Commun.*, 2004, **7**, 447–449.
27 J. -F. Chen, H. -M. Ding and J. -X. Wang, L. Shao, *Biomaterials*, 2004, **25**, 723–727.
28 Z. -Z. Li, S. -A. Xu, L. -X. Wen, F. Liu, A. -Q. Liu, Q. Wang, H. -Y. Sun, W. Yu and J. -F. Chen, *J. Controlled release*, 2006, **111**, 81–88.
29 J. Wang, H. Ding, X. Tao and J. Chen, *Nanotechnology*, 2007, **18**, 245705.
30 R. V. Rivera-Virtudazo, M. Fuji, C. Takai and T. Shirai, *Nanotechnology*, 2012, **23**, 485608.
31 T. Wang, F. Chai, Q. Fu, L. Zhang, H. Liu, L. Li, Y. Liao, Z. Su, C. Wang, B. Duan and D. Ren, *J. Mater. Chem.*, 2011, **21**, 5299–5306.
32 S. Liu, Z. Zhang, M. Han, *Adv. Mater.*, 2005, **17**, 1862–1866.
33 Y. Liu, H. Miyoshi and M. Nakamura, *Colloids Surf. B*, 2007, **58**, 180–187.
34 M. Darbandi, R. Thomann and T. Nann, *Chem. Mater.*, 2007, **19**, 1700–1703.
35 Y. -S., Lin, S. -H. Wu, C. -T. Tseng, Y. Hung, C. Chang and C. -Y. Mou, *Chem. Commun.*, 2009, 3542–3544.
36 S. -H. Wu, Y. Hung and C. -Y. Mou, *Chem. Mater.*, 2013, **25**, 352–364.
37 A. V. Jovanovic, R. S. Underhill, T. L. Bucholz and R. S. Duran, *Chem. Mater.*, 2005, **17**, 3375–3383.
38 H. Wang, Y. Wang, X. Zhou, L. Zhou, J. Tang, J. Lei and C. Yu, *Adv. Funct. Mater.*, 2007, **17**, 613–617.
39 B. Tan, H. -J. Lehmler, S. M. Vyas, B. L. Knutson and S. E. Rankin, *Adv. Mater.*, 2005, **17**, 2368–2371.
40 L. Zhang, P. Li, X. Liu, L. Du and E. Wang, *Adv. Mater.*, 2007, **19**, 4279–4283.
41 A. J. Karkamkar, S. -S. Kim, S. D. Mahanti and T. J. Pinnavaia, *Adv. Funct. Mater.*, 2004, **14**, 507–512.
42 D. H. W. Hubert, M. Jung, P. M. Frederik, P. H. H. Bomans, J. Meuldijk and A. L. German, *Adv. Mater.*, 2000, **12**, 1286–1290.
43 S. Yang, X. Zhou, P. Yuan, M. Yu, S. Xie, J. Zou, G. Q. Lu and C. Yu, *Angew. Chem. Int. Ed.*, 2007, **46**, 8579–8582.
44 B. Tan, S. M. Vyas, H. -J. Lehmler, B. L. Knutson and S. E. Rankin, *Adv. Funct. Mater.*, 2007, **17**, 2500–2508.
45 H. Djojoputro, X. F. Zhou, S. Z. Qiao, L. Z. Wang, C. Z. Yu and G. Q. Lu, *J. Am. Chem. Soc.*, 2006, **128**, 6320–6321.
46 J. Du, Y. Chen, Y. Zhang, C. C. Han, K. Fischer and M. Schmidt, *J. Am. Chem. Soc.*, 2003, **125**, 14710–14711.
47 M. Mandal and M. Kruk, *Chem. Mater.*, 2012, **24**, 123–132, and references therein.
48 X. Li, Y. Yang and Q. Yang, *J. Mater. Chem. A*, 2013, **1**, 1525–1535, and references therein.
49 K. Koh, K. Ohno, Y. Tsujii and T. Fukuda, *Angew. Chem. Int. Ed.*, 2003, **42**, 4194–4197.
50 J. -J. Yuan, O. O. Mykhaylyk, A. J. Ryan and S. P. Armes, *J. Am. Chem. Soc.*, 2007, **129**, 1717–1723.
51 Y. Li, J. Du and S. P. Armes, *Macromol. Rapid Commun.*, 2009, **30**, 464–468.
52 A. Khanal, Y. Inoue, M. Yada and K. Nakashima, *J. Am. Chem. Soc.*, 2007, **129**, 1534–1535.
53 Q. Huo, J. Liu, L. -Q. Wang, Y. Jiang, T. N. Lambert and E. Fang, *J. Am. Chem Soc.*, 2006, **128**, 6447–6453.
54 J. Liu, Q. Yang, L. Zhang, H. Yang, J. Gao and C. Li, *Chem. Mater.*, 2008, **20**, 4268–4275.
55 H. Tan, N. S. Liu, B. He, S. Y. Wong, Z. -K. Chen, X. Li and J. Wang, *Chem. Commun.*, 2009, 6240–6242.
56 H. Tan, J. M. Xue, B. Shuter, X. Li and J. Wang, *Adv. Funct. Mater.*, 2010, **20**, 722–731.
57 H. Tan, M. Wang, C. -T. Yang, S. Pant, K. K. Bhakoo, S. Y. Wong, Z. -K. Chen, X. Li and J. Wang, *Chem. Eur. J.*, 2011, **17**, 6696–6706.
58 B. Y. -W. Hsu, M. Wang, Y. Zhang, V. Vijayaragavan, S. Y. Wong, A. Y. -C. Chang, K. K. Bhakoo, X. Li and J. Wang, *Nanoscale*, 2014, **6**, 293–299.
59 Y. Zhang, M. Wang, Y. -G. Zheng, H. Tan, B. Y. -W. Hsu, Z. -C. Yang, S. Y. Wong, A. Y. -C. Chang, M. Choolani, X. Li and J. Wang, *Chem. Mater.*, 2013, **25**, 2976–2985.
60 H. Tan, Y. Zhang, M. Wang, Z. Zhang, X. Zhang, A. M. Yong, S. Y. Wong, A. Y.-C. Chang, Z. -K. Chen, X. Li, M. Choolani and J. Wang, *Biomaterials*, 2012, **33**, 237–246.
61 B. Y. -W. Hsu, C. Teh, H. Tan, S. Y. Wong, Y. Zhang, V. Korzh, X. Li and J. Wang, *RSC Adv.*, 2012, **2**, 12392–12399.
62 Y. Wan and S. -H. Yu, *J. Phys. Chem. C*, 2008, **112**, 3641–3647.
63 E. Yan, Y. Ding, C. Chen, R. Li, Y. Hu and X. Jiang, *Chem. Commun.*, 2009, 2718–2720.
64 L. Du, S. Liao, H. A. Khatib, J. F. Stoddart and J. I. Zink, *J. Am. Chem. Soc.*, 2009, **131**, 15136–15142.
65 R. K. Rana, Y. Mastai and A. Gedanken, *Adv. Mater.*, 2002, **14**, 1414–1418.
66 Y. Lu, H. Fan, A. Stump, T. L. Ward, T. Rieker and C. J. Brinker, *Nature*, 1999, **398**, 223–226.
67 P. Tartaj, T. González-Carreño and C. J. Serna, *Adv. Mater.*, 2001, **13**, 1620–1624.
68 X. Fang, X. Zhao, W. Fang, C. Chen and N. Zheng, *Nanoscale*, 2013, **5**, 2205–2218, and references therein.
69 M. Roca and A. J. Haes, *J. Am. Chem. Soc.*, 2008, **130**, 14273–14279.
70 D. Chen, L. Li, F. Tang and S. Qi, *Adv. Mater.*, 2009, **21**, 3804–3807.
71 Y. Yang, J. Liu, X. Li, X. Liu and Q. Yang, *Chem. Mater.*, 2011, **23**, 3676–3684.

72 Y. Chen, H. Chen, L. Guo, Q. He, F. Chen, J. Zhou, J. Feng and J. Shi, *ACS Nano*, 2010, **4**, 529–539.
73 W. -K. Oh, S. Kim, M. Choi, C. Kim, Y. S. Jeong, B. -R. Cho, J. -S. Hahn and J. Jang, *ACS Nano*, 2010, **4**, 5301–5313.
74 M. Choi, C. Kim, S. O. Jeon, K. S. Yook, J. Y. Lee and J. Jang, *Chem. Commun.*, 2011, **47**, 7092–7094.
75 X. Jiang and C. J. Brinker, *J. Am. Chem. Soc.*, 2006, **128**, 4512–4513.
76 X. Wu and C. M. Crudden, *Chem. Mater.*, 2012, **24**, 3839–3846.
77 X. -J. Wu and D. Xu, *J. Am. Chem. Soc.*, 2009, **131**, 2774–2775.
78 D. Niu, X. Liu, Y. Li, Z. Ma, W. Dong, S. Chang, W. Zhao, J. Gu, S. Zhang and J. Shi, *J. Mater. Chem.*, 2011, **21**, 13825–13831.
79 Y. Jiao, J. Guo, S. Shen, B. Chang, Y. Zhang, X. Jiang and W. Yang, *J. Mater. Chem.*, 2012, **22**, 17636–17643.
80 J. Kim, J. E. Lee, J. Lee, J. H. Yu, B. C. Kim, K. An, Y. Hwang, C. -H. Shin, J. -G. Park, J. Kim and T. Hyeon, *J. Am. Chem. Soc.*, 2006, **128**, 688–689.
81 X. Jiang, T. L. Ward, Y. -S. Cheng, J. Liu and C. J. Brinker, *Chem. Commun.*, 2010, **46**, 3019–3021.
82 D. Niu, Y. Li, Z. Ma, H. Diao, J. Gu, H. Chen, W. Zhao, M. Ruan, Y. Zhang and J. Shi, *Adv. Funct. Mater.*, 2010, **20**, 773–780.
83 Y. -K. Peng, C. -W. Lai, C. -L. Liu, H. -C. Chen, Y. -H. Hsiao, W. -L. Liu, K. -C. Tang, Y. Chi, J. -K. Hsiao, K. -E. Lim, H. -E. Liao, J. -J. Shyue and P. -T. Chou, *ACS Nano*, 2011, **5**, 4177–4187.
84 T. Kim, E. Momin, J. Choi, K. Yuan, H. Zaidi, J. Kim, M. Park, N. Lee, M. T. McMahon, A. Quinones-Hinojosa, J. W. M. Bulte, T. Hyeon and A. A. Gilad, *J. Am. Chem. Soc.*, 2011, **133**, 2955–2961.
85 M. Yu, S. Karmakar, J. Yang, H. Zhang, Y. Yang, P. Thornb and C. Yu, *Chem. Commun.*, 2014, **50**, 1527–1529.
86 J. Zhu, J. Tang, L. Zhao, X. Zhou, Y. Wang and C. Yu, *Small*, 2010, **6**, 276–282.
87 J. Peng, L. Zhao, X. Zhu, Y. Sun, W. Feng, Y. Gao, L. Wang, F. Li, *Biomaterials*, 2013, **34**, 7905–7912.

Table of Contents Entry

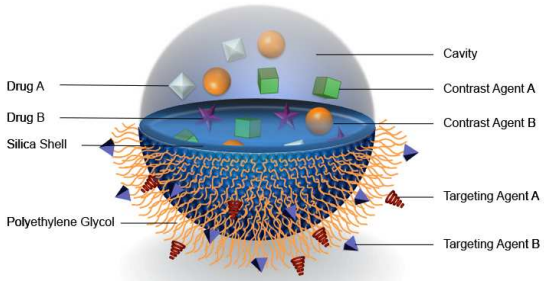

Synthesis and structure engineering of silica-based nanocapsules for biomedical applications.